CB2R-induced differentiation epigenetically restrains cancer plasticity enabling adaptive therapy

Nuria G. Martínez-Illescas[1,2], Gemma Pérez-García[1], María Rubert-Hernández[2,3], Camila Quezada-Gutiérrez[1], Estrella Martín-Zapater[1], Luis M. Alonso-Colmenar[4], Carmen Hernández[4], Ángela Zarco-Cuadrillero[5], Eduardo Caleiras[6], Miguel Muñoz-Ruiz[5], Ana Payo-Payo[7], Laura Frías-Aldeguer[8], Cristina Sánchez[2,3], Mercedes Balcells-Camps[9,10], Elazer R. Edelman[9], María Salazar-Roa[1,2]*

1 Cancer STEM Lab, Dept. Biochemistry and Molecular Biology, Faculty of Biological Sciences, Complutense University (UCM), Madrid, Spain

2 Breast and Gynecologic Cancer Group, Research Institute i+12; Madrid, Spain

3 Dept. Biochemistry and Molecular Biology, Faculty of Biological Sciences, UCM, Madrid, Spain

4 Flow Cytometry and Fluorescence Microscopy Unit, UCM, Madrid, Spain

5 Dept. Immunology, Faculty of Medicine, UCM, Madrid, Spain

6 Histopathology Unit, Spanish National Cancer Research Center, Madrid, Spain

7 Animal Ecology Lab, Dept. Biodiversity, Ecology and Evolution, Faculty of Biological Sciences, UCM, Spain

8 Mammary Pathology Unit, Hospital La Paz, Madrid, Spain

9 Harvard-MiT Biomedical Engineering Center, MIT Institute for Medical Engineering and Science, Cambridge, US

10 Instituto Químico de Sarriá (IQS), School of Engineering, Ramon Llull University, Barcelona, Spain

**Correspondence should be addressed to María Salazar-Roa (mariasalazarroa@ucm.es)*

Running title: *CB2R drives cancer differentiation*.

Abstract

Tumor adaptability relies on the ability of cancer cells to dedifferentiate and acquire stem-like features, fueling therapeutic resistance and metastasis. Differentiation therapy aims to reprogram tumor cells into more mature, less aggressive states to counteract this plasticity. Here, we identify cannabinoid receptor 2 (CB2R) as a novel therapeutic target that promotes sustained differentiation in breast cancer.

Using tumor-derived organoids from both mouse models and patient biopsies, we show that brief, low-dose exposure to phytogenic or synthetic CB2R ligands induces a basal-to-luminal switch, suppresses stemness, and reduces invasiveness and self-renewal. These phenotypic changes are associated with decreased tumor initiation and aggressiveness *in vivo*. Transcriptomic profiling reveals that CB2R activation initiates transient chromatin remodeling and epigenetic reprogramming, resulting in a stably differentiated state.

Importantly, CB2R-driven differentiation sensitizes tumor cells to tamoxifen, enabling lower therapeutic doses with improved efficacy—supporting the principles of adaptive therapy aimed at long-term disease control. Our findings position CB2R modulation as a promising non-cytotoxic strategy to restrict cancer plasticity and enhance the effectiveness of existing breast cancer treatments.

Introduction

Recent evidence of cellular plasticity and spontaneous de-differentiation suggests that cancer developmental landscape is far more complex than a simple hierarchical structure. “Phenotypic plasticity,” a newly recognized hallmark of cancer, plays a significant role in this complexity (1). Traditional cancer treatments, such as cytotoxic drugs and radiotherapy, primarily aim to target cell division through mechanisms of widespread cell damage and toxicity. However, these approaches often prove inefficient and may create evolutionary pressures that favor the emergence of aggressive, resistant cancer clones. In some cases, cytotoxic treatments even promote undesirable side effects, such as metastasis.

In contrast, differentiation therapies aim to induce terminal differentiation in cancer cells, effectively removing them from the proliferative compartment (2, 3). By promoting differentiation in a subset of tumor cells, these therapies can alter tumor dynamics by limiting the growth potential of the entire tumor. This effect is akin to habitat fragmentation, where differentiated cells occupy space and resources that would otherwise be used for tumor expansion, thereby restricting the carrying capacity. Notably, when differentiation strategies are combined with cytotoxic therapies, tumor dynamics can shift from growth to regression (3).

Tumors with high stem cell traits are, therefore, ideal candidates for differentiation-based and potentially, combined therapies. The mammary gland, a tissue characterized by significant postnatal development and cyclical expansion, exhibits considerable stem cell plasticity. This plasticity is particularly relevant in the context of poorly differentiated breast carcinomas, which are known for their rapid spread and high incidence of metastasis, making them a major challenge in cancer treatment. Indeed, a significant proportion of breast cancer-related deaths are attributed to relapse or dissemination after surgery/therapy, a phenomenon most commonly observed in patients with poorly differentiated tumors (4). While the direct relationship between tissue differentiation and partial pathologic complete response (pCR) after treatments remains unclear (5, 6), existing correlations emphasize the need of differentiation-based treatment approaches.

Designing effective differentiation therapies requires an understanding of the parallels between cancer and embryonic development. Many signalling pathways involved in embryogenesis are aberrantly reactivated in cancer, with genetic and epigenetic changes driving this process (7-11). These pathways, including Wnt/β-catenin (12), Hedgehog (Hh) (13), Notch

75 (14), TGF-β (15), PI3K /AKT (16) and JAK/STAT (17), govern cellular differentiation during normal
76 development. In cancer, their reactivation contributes to disease pathology, driving the
77 reprogramming of tumor cells to a progenitor-like state—a key feature of metastasis. Notably, the
78 endocannabinoid system (ECS) has been shown to regulate many of these pathways (18).

79 The ECS is a complex cellular network that regulates a variety of physiological functions
80 (19, 20). It consists of two main cannabinoid receptors, CB1R and CB2R, their endogenous
81 ligands (AEA and 2-AG), and associated proteins responsible for their synthesis, transport, and
82 degradation. Over the past two decades, substantial evidence has demonstrated that ECS
83 activation has anti-tumor effects in cell and animal models, including promoting tumor cell death,
84 inhibiting endothelial cell migration, blocking tumor angiogenesis, and suppressing tumor cell
85 adhesion and migration (21, 22). Much of this research has focused on cannabinoids derived
86 from *Cannabis sativa*, which contains over 500 compounds, including the primary cannabinoids
87 Δ9-tetrahydrocannabinol (THC) and cannabidiol (CBD) (23). Additionally, synthetic cannabinoid
88 receptor ligands have shown similar effects in cancer models (24). These findings have prompted
89 clinical trials investigating the safety and efficacy of cannabinoids as anti-tumor agents (25-28).

90 In this study, we expand the therapeutic potential of cannabinoids by exploring their use
91 as differentiation drivers in cancer. Using three-dimensional organoids derived from breast cancer
92 mouse models and patient biopsies, we demonstrate that both natural and synthetic Cannabinoid
93 Receptor 2 (CB2R) ligands promote long-term and stable tumor cell differentiation when
94 administered at low doses (nanomolar concentrations) and short treatment regimens (4 days
95 followed by drug withdrawal). Moreover, combining these differentiation strategies with
96 tamoxifen—a widely used breast cancer treatment—significantly enhances therapeutic outcomes
97 while allowing for reduced chemotherapy doses and exposure, thus mitigating undesirable side
98 effects.

99 **Results**

100 **Low-dose, transient THC exposure durably reprograms mammary tumor organoids,**
101 **disrupting cancer cell plasticity *in vitro* and *in vivo*.**

102 Cannabinoids have been widely studied for their anti-tumor properties—suppressing
103 proliferation, invasion, metastasis, and promoting autophagy and cell death [recently reviewed in
104 (18)]. However, their role in regulating tumor differentiation remains poorly understood. Since
105 differentiation therapies align with adaptive treatment strategies aimed at reducing tumor
106 evolution and resistance (29), we first examined whether low-dose THC could durably modulate
107 tumor cell plasticity.

108 To test this, we exposed MMTV-PyMT mammary tumor organoids to nanomolar vs.
109 micromolar concentrations of THC. While high doses triggered expected cytotoxic effects, 10 nM
110 THC induced significant long-term morphological and molecular changes exclusively in 3D
111 cultures, but not in 2D (**Supp. Fig. 1**). Based on this, we developed a protocol using a 4-day 10
112 nM THC pulse, followed by extended drug-free culture (**Fig. 1A**). Strikingly, this short, low-dose
113 exposure consistently induced a basal-to-luminal switch, both morphologically (**Fig. 1B–E**) and
114 at the molecular level (**Fig. 1F–G**), highlighting a stable reprogramming effect on tumor cell
115 identity. These effects were replicated in organoids derived from MMTV-Her2/neu tumors (**Supp.**
116 **Fig. 2**), confirming that THC-driven differentiation is not model-specific. Functionally, THC
117 treatment inhibited collective migration, triggered a mesenchymal-to-epithelial transition (MET)
118 (**Fig. 2A–D**), and reduced stem-like features and self-renewal capacity (**Fig. 2E–G**). These
119 phenotypes were also validated in patient-derived breast cancer organoids (**Supp. Fig. 3**),
120 underscoring their potential clinical relevance.

121 To assess functional *in vivo* consequences, THC-treated and control organoids were
122 orthotopically injected into wild-type PyMT mice (**Fig. 3A–B**). THC-pretreated organoids showed
123 markedly reduced tumor initiation capacity, and the few tumors that did form exhibited delayed
124 growth and non-malignant histology, in contrast to controls which developed aggressive
125 neoplasias (**Fig. 3C–E**). In tail-vein injection assays, THC-pretreated organoids produced
126 significantly fewer lung micro- and macro-metastases compared to controls (**Fig. 3F–I**).

127 Together, these findings reveal that brief, low-dose THC exposure durably reprograms
128 tumor cell fate, reducing plasticity, stemness, and metastatic potential both *in vitro* and *in vivo*.

129 **CB2 receptor mediates cannabinoid-induced differentiation in breast cancer organoids.**

130 To explore the role of cannabinoid receptor tone in tumor cell differentiation, we
131 compared the effects of pure phytocannabinoids (THC, CBD), *Cannabis sativa* extracts, and
132 methanandamide (mAEA)—a metabolically stable analog of the endocannabinoid AEA—on
133 MMTV-PyMT-derived mammary tumor organoids. As shown in **Supplementary Fig. 4**, both
134 extracts and pure cannabinoids induced similar morphological changes, reduced collective
135 migration, and promoted a basal-to-luminal molecular switch. In contrast, mAEA did not equally
136 influence differentiation, maybe due to its low affinity for CB2R. We next assessed synthetic
137 inverse agonists of cannabinoid receptors: SR1 (CB1R) and SR2 (CB2R). Interestingly, SR2, but
138 not SR1, recapitulated THC effects—inducing durable basal-to-luminal reprogramming, inhibiting
139 migration (**Fig. 4A–E**), and reducing self-renewal (**Fig. 4F**). This unexpected finding suggested a
140 functional role for CB2R in regulating tumor plasticity. Combining THC with either SR1 or SR2 did
141 not block its long-term effects on morphology, migration, or organoid size (**Supp. Fig. 5A–D**),
142 implying that CB2R modulation is sufficient but not necessarily required for THC-mediated
143 reprogramming. Supporting this, CB2R expression modestly increased following cannabinoid
144 treatment in differentiation-responsive contexts (**Supp. Fig. 5E**).

145 To directly test the role of CB2R, we generated CB2R knockout mice (MMTV-PyMT
146 CB2R^{-}/$^{-}$). These mice developed tumors with delayed onset compared to wild-type controls
147 (**Supp. Fig. 6A**), consistent with previous observations in other models (30). CB2R deficiency
148 also altered tumor biology—lower Ki67 and SOX gene expression suggested reduced
149 proliferation and stemness (**Supp. Fig. 6B**). While flow cytometry revealed no major shifts in
150 EpCAM/CD49f-defined subpopulations between CB2R^{-}/$^{-}$ and WT tumors (**Supp. Fig. 6C**), the
151 capacity to form viable organoids from luminal progenitors was significantly impaired in CB2R^{-}/$^{-}$
152 mice (**Supp. Fig. 6D**). Additionally, CB2R knockout organoids exhibited distinct basal-like
153 morphologies, reduced size, diminished collective migration, and decreased long-term self-
154 renewal (**Supp. Fig. 6E–J**), closely resembling the phenotype induced by THC and SR2.

155 Together, these findings identify CB2R signaling as a key modulator of tumor
156 differentiation, capable of driving durable reprogramming in breast cancer organoids.

157

158 **THC and SR2 trigger an early, transient epigenetic reprogramming in breast cancer**
159 **organoids, driving sustained cellular differentiation.**

160 Cellular differentiation is tightly linked to epigenetic remodeling, yet the connection
161 between CB2R signaling and epigenetic regulation in cancer remains poorly defined (18). To
162 investigate this relationship, we conducted transcriptomic profiling of mammary tumor organoids
163 treated with THC or SR2, focusing on genes related to epigenetic control and stemness. As shown
164 in **Figure 5**, both treatments triggered a distinct, phase-specific gene expression program. By day
165 3, organoids displayed a transcriptional signature enriched for embryonic and pluripotency-
166 associated genes (**Fig. 5A–D**), reminiscent of the early reprogramming stages observed in ESCs
167 and iPSCs. This transient increase in plasticity was followed by a clear shift toward a
168 differentiation-related transcriptional profile at later time points (**Fig. 5E**), underscoring a
169 structured reprogramming process.

170 Gene set enrichment and differential expression analyses revealed broad modulation of
171 epigenetic regulators involved in histone modifications, chromatin remodeling, and DNA
172 methylation (**Fig. 5C**). These changes aligned with increased accessibility at bivalent chromatin
173 domains (**Fig. 5D, 5F, 5G**), suggesting that CB2R signaling may facilitate transcriptional priming
174 and epigenetic poising of differentiation programs. Indeed, among the top transiently expressed
175 genes, Utf1 emerged as particularly notable—a key regulator of Polycomb Repressive Complex
176 (PRC) activity and pluripotency maintenance (31, 32). Utf1 was upregulated early after THC or
177 SR2 exposure, and subsequently downregulated at later stages, reflecting the transition from a
178 plastic to a more differentiated state (**Fig. 5B**). Consistent with this, the expression of *bona-fide*
179 UTF1 and PRC2 target genes was synchronously modulated under our experimental conditions
180 (**Fig. 5F–G**). Furthermore, we confirmed bivalent histone marks in organoids treated with THC
181 and SR2, which indeed induced a balanced ratio of H3K27me3/ H3K4me3, reinforcing the role of
182 bivalent chromatin regulation in establishing and maintaining cannabinoid-induced differentiation
183 programs (**Fig. 5H–I)**.

184 Together, these results demonstrate that short-term CB2R activation triggers a transient
185 epigenetic reset, effectively priming mammary tumor organoids for long-term, stable
186 differentiation.

187

188 **CB2R-driven differentiation locks tumor cells into a stable, irreversible phenotype.**

189 A critical limitation of current differentiation therapies is their potential reversibility,
190 especially under microenvironmental pressures that favor stemness and aggressiveness (2). To
191 challenge the stability of CB2R-induced differentiation, we developed a dynamic co-culture
192 system mimicking a pro-tumorigenic niche. This system included cancer-associated fibroblasts
193 (CAFs), peripheral blood mononuclear cells (PBMCs), and continuous shear stress via a flow-
194 controlled bioreactor (**Fig. 6A and Supp. Fig. 7**). As expected, co-culture with CAFs significantly
195 enhanced tumor cell migration, and reinforced basal and mesenchymal traits in tumor organoids
196 (**Supp. Fig. 7A–E**). These effects, along with a significant increase in organoid size, were further
197 amplified by the inclusion of PBMCs and shear stress (**Supp. Fig. 7F–J**), confirming the model's
198 capacity to promote cellular plasticity and invasive behavior. Remarkably, even under these
199 challenging microenvironmental conditions, both THC and SR2 treatments effectively
200 reprogrammed tumor organoids toward a luminal, differentiated state and maintained this
201 phenotype over time (**Fig. 6B–E**). Notably, this differentiation state persisted despite prolonged
202 exposure to CAFs, PBMCs, and shear stress, highlighting the durability of cannabinoid-induced
203 reprogramming. To note, cytokine profiling revealed that SR2- and THC-treated co-cultures
204 exhibited a broad activation of immune responses and a reduction in chemokines associated with
205 tumor progression (**Fig. 6F**). Furthermore, cannabinoid-treated organoids displayed sustained
206 epigenetic remodeling, as described above, even within this aggressive microenvironment (**Fig.
207 6G–H**).

208 Collectively, these results demonstrate that CB2R modulation triggers a robust,
209 irreversible differentiation program capable of resisting pro-aggressive cues—supporting its
210 potential as a therapeutic strategy to counteract the inherent plasticity of breast cancer cells.

211

212 **CB2R-driven differentiation sensitizes breast cancer cells to endocrine therapy.**

213 Drug-resistant cancer cells often incur a fitness cost—reduced growth, higher metabolic
214 demands, or lower competitiveness. Adaptive therapy exploits this trade-off by maintaining a
215 population of drug-sensitive cells to suppress resistant clones through natural competition, thus
216 delaying resistance and improving long-term outcomes (33). In this framework, differentiation
217 therapies, including CB2R-targeted strategies, may act as adaptive interventions by reducing

218 tumor stemness and plasticity, thereby lowering resistance potential. To explore this therapeutic
219 synergy, we tested CB2R-mediated differentiation followed by tamoxifen, a widely prescribed
220 endocrine therapy for ER^+ breast cancer (34) (**Fig. 7A**). Transcriptomic profiling revealed that
221 both THC and SR2 treatments significantly enhanced estrogen signaling pathways (**Fig. 5E**),
222 providing a rationale for their combination with tamoxifen. Organoids were first exposed to CB2R
223 ligands for 4 days, and ten days after drug withdrawal, treated with sub-micromolar concentrations
224 of tamoxifen for 4 days. This sequential combination therapy led to reduced cell viability (**Fig. 7B**)
225 and G2-M cell cycle arrest (**Fig. 7C**) in cannabinoid-pretreated organoids. After 4 weeks of drug
226 withdrawal, these first observations translated into a more pronounced basal-to-luminal shift (**Fig.**
227 **7D**), smaller organoid size (**Fig. 7E**), impaired collective migration (**Fig. 7F**) and particularly
228 relevant, reduced long-term self-renewal (**Fig. 7G**). Importantly, CB2R-based pretreatment
229 completely abolished the emergence of resistant clones, which were evident in tamoxifen-only
230 cultures (**Fig. 7G**). This demonstrates that cannabinoid-induced differentiation not only sensitizes
231 tumor cells to endocrine therapy but also prevents adaptive resistance.

232 To validate these observations in clinically relevant settings, we tested the combinatory
233 treatment in patient-derived samples. Surgical specimens from two breast tumors were processed
234 for organoid culture, and the efficacy of the SR2–tamoxifen regimen was assessed following the
235 experimental timeline outlined in **Fig. 8A**. Using phase holographic imaging, we analyzed cancer
236 cell movement and dispersal 10 days after CB2R-based differentiation. Cells pretreated with SR2
237 exhibited reduced motility, altered migration directionality, and changes in cell area and shape
238 irregularity, suggesting impaired adaptation for migration (**Fig. 8B–F and Supp. Fig. 8**). At this
239 same time point, SR2 treatment had also enhanced cell–cell adhesion within the 3D organoids,
240 as evidenced by increased E-cadherin and decreased Snail expression (**Fig. 8G**), along with a
241 marked reduction in organoid size (**Fig. 8H**) and diminished collective migration (**Fig. 8I**).
242 Following this, organoid cultures were exposed to 5 μM tamoxifen for 4 days. Notably, the
243 differentiated cellular state induced by SR2 created a highly favorable context for tamoxifen
244 therapy: organoids pretreated with SR2 showed severely impaired self-renewal following
245 tamoxifen exposure, whereas control organoids retained normal self-renewal capacity despite
246 tamoxifen treatment (**Fig. 8J–K**).Together, these results highlight the potential of CB2R

modulation as a priming strategy to enhance the efficacy of standard treatments, aligning with adaptive therapy principles to improve durable cancer control.

Discussion

Cancer cells undergo numerous molecular and behavioral changes that enable them to overcome natural selection barriers, one of the most notable being the loss of differentiation markers and a reprogramming to a de-differentiated state. This reversion to an earlier developmental stage provides the tumor with increased plasticity and self-renewal capacity.

The standard treatment for cancer traditionally relies on cytotoxic drugs and radiotherapy, both of which induce cell damage and death, especially in highly proliferative cells. However, these therapies are often criticized for their side effects and their tendency to trigger evolutionary pressures, leading to the emergence of resistant and aggressive tumor clones. As a result, there is growing interest in integrating additional therapeutic approaches, including personalized medicine and immune-directed therapies, to improve clinical outcomes. Among the most promising alternatives to cytotoxic treatments are differentiation therapies, which, although proposed over 50 years ago (35) are still being explored. The principle behind these therapies is that cancer cells, to expand and maintain plasticity, often block differentiation processes. Differentiation therapy does not aim to induce cell death but instead focuses on inhibiting self-renewal and guiding tumor cells back toward terminal differentiation.

One of the most successful examples of differentiation therapy is the treatment of Acute Promyelocytic Leukaemia (APL), where a combination of cytotoxic therapy and all-trans retinoic acid (RA) has dramatically improved remission rates and survival outcomes (36, 37). Notably, while RA alone induces high differentiation grades, long-term disease remission is not achieved, suggesting that combination therapies yield the best results. In solid tumors, differentiation therapy is still in its early stages but remains a promising second-line option for patients with advanced cancer.

Our study uncovers a previously unrecognized role for the cannabinoid receptor CB2 (CB2R) in driving stable cancer cell differentiation in breast cancer. We show that a brief, low-dose exposure to THC or the CB2R ligand SR2 durably reprograms mammary tumor organoids,

triggering a basal-to-luminal switch, reducing stemness, and impairing migration, self-renewal, and metastatic potential—effects that persist *in vitro* and *in vivo*.

Over the past decades, substantial preclinical and clinical evidence has demonstrated that the endocannabinoid system (ECS) regulates several physiological functions, including pain perception, motor coordination, and nausea/vomiting (38), common side effects of chemotherapy. Our lab was among the pioneers in documenting the anti-tumor properties of cannabinoids (39), showing their ability to block proliferation, migration, and angiogenesis (22). These findings laid the groundwork for the first phase 1b randomized, placebo-controlled clinical trial assessing the effects of the cannabis-based drug Sativex on tumor progression in patients with recurrent glioblastoma. This trial demonstrated the safety, tolerability, and lack of interaction with temozolomide (the standard treatment), as well as a notable survival benefit at one year (27). With the increasing legalization of cannabis in over 80 countries, there has been a growing interest in its clinical applications, particularly in cancer treatment.

Our study contributes to the expanding body of research on cannabinoids in cancer therapy by focusing on a relatively unexplored application: While cannabinoids have been implicated in nearly all cancer hallmarks (40), their role in differentiation has received less attention. Previous studies, particularly in leukaemia, have shown that THC can sensitize cancer cells to chemotherapeutic agents, reducing IC50 values by approximately 50% and enhancing overall therapeutic effects (41). Additionally, Dronabinol, an FDA-approved cannabinoid, has been shown to inhibit differentiation blockage in acute leukaemia cells (42). In myelomas, THC has been found to induce differentiation of myeloid-derived suppressor cells, reducing immune evasion (43). Most studies have used cannabinoid concentrations in the micromolar range (1-25 μM) (44, 45), with effects typically observed after prolonged exposure. In contrast, our study is the first to evaluate the anti-cancer effects of cannabinoids at nanomolar concentrations (10 nM) in three-dimensional organoid models derived from both mouse and human solid tumors. Moreover, we assess the long-term impact of a brief cannabinoid exposure (4 days), followed by drug withdrawal for at least two weeks, a novel approach that has not been previously explored. Significantly, this work also shows that, after cannabinoid treatment, tumors can be subjected to chemotherapy at reduced doses, resulting in improved therapeutic outcomes. Therefore, our data

306 illustrate a new potential practice of adaptive therapy, with important implications in tumor cell
307 plasticity and relapse impairment.

308 Intriguingly, we found that THC, SR2, and CB2 receptor knockout (CB_2KO) cells exhibit
309 similar effects on cancer cell differentiation. Although THC is known to be a partial agonist at both
310 CB1 and CB2 receptors (46) and SR2 is an inverse agonist of CB2R, THC may act also as an
311 inverse agonist at CB2 receptors in a stemness context, or its brief and low-dose exposure might
312 stimulate a CB2-CB1 receptor switch, similar to what has been observed in neuronal
313 differentiation (47-49). This hypothesis aligns with the idea that CB2 receptors are overexpressed
314 in cancer, contributing to tumor aggressiveness, and that cancer differentiation would involve the
315 downregulation of CB2 receptors and a (potential) subsequent upregulation of CB1 receptors
316 (50). Those exciting possibilities are out of the scope of this work but deserve broader research.

317 Our work shows that brief exposure to CB2R ligands such as THC or SR2 significantly
318 enhances the long-term differentiation potential of cancer cells, even after multiple passages,
319 suggesting an epigenetic mechanism. In fact, RNAseq analyses revealed and early remodeling
320 of the epigenetic landscape, apparently establishing a form of replication memory, that promoted
321 a sustained differentiated state several weeks after treatment. Among the top genes regulated by
322 THC or SR2, Undifferentiated Transcription Factor 1 (UTF1) likely plays an important role in this
323 effect. Extensive research supports its function as a central mediator of epigenetic stability, both
324 in early embryogenesis (51), governing lineage specification, and in cancer, when it has been
325 showed to bind chromatin with histone-like dynamics, maintaining nuclear structure during cell
326 fate transitions (31, 52, 53). Mechanistically, UTF1 localizes to promoters of developmental
327 genes—particularly those that are silenced or bivalently marked (e.g., H3K4me3 and H3K27me3),
328 fine tuning the balance between self-renewal and differentiation (32). Indeed, its expression
329 diminishes as cells begin to differentiate. Collectively, these findings position UTF1 potentially
330 explaining the long-term effects of transient CB2R ligand exposure on cancer cell differentiation.

331 Synthetic CB2R ligands have shown great promise in pharmacological research, with
332 conceivable applications in neurodegenerative diseases, autoimmune disorders, chronic pain,
333 and cancer (54). However, clinical testing of CB2R-targeted compounds is still in its early stages.
334 Our findings provide strong support for the therapeutic potential of SR2 as differentiation agent in
335 cancer, since our data show that SR2-treated organoids exhibit even stronger differentiation

336 effects than those treated with THC. These results, combined with recent advances in CB2R
337 pharmacology, suggest a promising future for CB2R synthetic ligands in novel cancer therapy.
338
339 **Methods**
340
341 ***Animal models and procedures***
342 All animal procedures were approved by the Animal Experimentation Committee of the
343 Complutense University of Madrid (CEIyBA) and the Regional Government of Madrid, in
344 compliance with European animal research regulations. Mice were housed under a 12-hour
345 light/dark cycle with ad libitum access to food and water. PyMT mice [FVB/N-Tg(MMTV-
346 PyMT)$^{634Mul/J}$] were generously provided by Miguel Quintela (CNIO, Spain). The MMTV-
347 neu:CB2R$^{-/-}$ strain was previously developed in our laboratory (30) and MMTV-neu [FVB/N-
348 Tg(MMTV-neu)$^{202Mul/J}$] mice were obtained by selecting CB2R$^{+/+}$ individuals from this colony. To
349 generate the PyMT:CB2R$^{-/-}$ line, PyMT mice were crossed with MMTV-neu:CB2R$^{-/-}$ mice. The
350 CB2R$^{-/-}$ allele was introduced through four generations of backcrossing, during which the neu
351 transgene was also eliminated. Genotyping was performed using the following primers (5′−3′; F:
352 forward, R: reverse). **PyMT**, F: TGC CGG GAA CGT TTT ATT AG; R: GGA ACA AGT ACC CCA
353 GCT CA; **CB2R-WT/KO**, F: CTA CAA AGC TCT AGT CAC CCG; WT-R: GGC TCC TAG GTG
354 GTT TTC ACA TCA GCC TCT; KO-R: CTA AAG CGC ATG CTC CAG AC; **Neu**, F: GCT CAG
355 AGA CCT GCT TTG GA; R: AGG AGG ACG AGT CCT TGT AGT G. PCR was performed using
356 the following protocol: 95 °C for 15 min; 30 cycles of 94 °C for 30 s, 63 °C for 45 s, 72 °C for 1 min;
357 final extension at 72 °C for 10 min; hold at 4 °C.
358
359 ***Reagents***
360 Cannabinoid-based treatments included Δ⁹-tetrahydrocannabinol (THC, THC Pharm),
361 cannabidiol (CBD), methanandamide (mAEA, Cayman Chemical, #90050), a high-THC cannabis
362 extract, and a balanced THC:CBD (1:1) extract (kind gift from Dr. Paola Pineda, Grupo Curativa,
363 Colombia). Selective cannabinoid receptor inverse agonists included SR141716A (CB1R, SR1,
364 Tocris Bioscience, #0923) and SR144528 (CB2R, SR2, Tocris Bioscience, #1464). Tamoxifen
365 (Sigma, T5648) was used as a reference endocrine therapy. Stock solutions were prepared for a
366 final 1:1000 dilution. mAEA was dissolved in ethanol; all other compounds (THC, CBD, extracts,

367 SR1, SR2, and tamoxifen) were dissolved in DMSO. Vehicle controls were included in all
368 experiments using matched volumes of the respective solvents (DMSO or ethanol) in the culture
369 medium.
370
371 ***Primary tumor cell isolation and culture***
372 PyMT mice were euthanized at 6–8 weeks of age upon development of palpable tumors.
373 Tumors were excised and placed on ice in tumor cell medium consisting of DMEM (Corning, 10-
374 017-CV) supplemented with 1× GlutaMAX (Invitrogen, 12634-034), 10% FBS (Gibco, A5256701),
375 and antibiotics. Under aseptic conditions, tumors were minced into small fragments using a sterile
376 scalpel. Minced tissue was incubated in 5 mL of freshly prepared digestion solution (tumor
377 medium supplemented with 0.125 mg/mL Collagenase [Sigma, C9407] and 0.125 mg/mL Dispase
378 II [Gibco, 17105041]), prewarmed to 37 °C. The suspension was digested at 37 °C with agitation
379 (150 rpm) for 2 hours. Post-digestion, the mixture was filtered through a 100 μm cell strainer to
380 remove debris, centrifuged at 400 x g, and resuspended in fresh tumor medium. Cells were plated
381 and incubated at 37 °C for 20 minutes to promote adherence. Non-adherent cells were removed
382 by washing to eliminate fibroblasts and stromal contaminants. Fresh medium was then added.
383 Primary tumor cells were confirmed as epithelial by positive staining for pan-cytokeratin (Abcam,
384 ab7753). Cultures were maintained at 37 °C in a humidified incubator with 5% CO_2, tested weekly
385 for mycoplasma contamination, and passaged every 4 days upon reaching confluence.
386
387 ***Generation and culture of mammary tumor organoids***
388 PyMT, PyMT:CB2R^{-}/$^{-}$, and MMTV-neu mice were euthanized at 6–8 weeks of age, and
389 tumors were harvested for organoid generation. Organoids were established and maintained as
390 previously described (5). Briefly, excised tumors were minced and digested in pre-warmed
391 digestion solution consisting of DMEM supplemented with 1× GlutaMAX, 1% FBS, antibiotics
392 (referred to as wash medium), 0.125 mg/mL collagenase, and 0.125 mg/mL Dispase II. The tissue
393 suspension was incubated at 37 °C with constant shaking (150 rpm) for 2 hours. Following
394 enzymatic digestion, the cell suspension underwent sequential centrifugation at 500 × g to wash
395 away adipose tissue remnants using cold wash medium. The resulting pellet was resuspended in
396 basal medium composed of Advanced DMEM/F-12 (Invitrogen, 12634-034), 1× GlutaMAX, 10

397 mM HEPES (Invitrogen, 15630-056), and antibiotics, then centrifuged again at 500 × g. Pellets
398 were carefully resuspended in 10 mg/mL cold Cultrex growth factor-reduced Basement
399 Membrane Extract (BME) Type 2 (Trevigen, 3533-010-02), and 40 µL domes were plated in pre-
400 warmed 24-well plates. After the BME solidified, 650–1000 µL of pre-warmed breast cancer (BC)
401 organoid expansion medium was added to each well. The expansion medium was prepared by
402 supplementing the basal medium with the following components: 10% homemade R-Spondin-1
403 conditioned medium, 1× B27 supplement (Gibco, 17504-044), 1× N2 supplement (Gibco, 17-502-
404 001), 10 mM nicotinamide (Sigma, N0636), 1.25 mM N-acetylcysteine (Sigma, A9165), 10 nM
405 Gastrin I (Sigma, G9145), 100 ng/mL FGF10 (Peprotech, 100-26), 50 ng/mL Noggin (Peprotech,
406 120-10C), 50 ng/mL EGF (Peprotech, AF-100-15), 5 nM Neuregulin-1 (Peprotech, 100-03), 5 µM
407 Y-27632 (Abmole), 500 nM A83-01 (Tocris, 2939), 500 nM SB202190 (Sigma, S7067), and
408 Primocin (Invitrogen, Ant-pm-1). Organoids were passaged weekly, and expansion medium was
409 refreshed every two days. For cannabinoid treatment, organoids were exposed for four days to
410 compounds dissolved in DMSO at the following concentrations: 1 nM to 5 µM Δ9-THC, 10 nM
411 CBD, 10 nM THC-rich plant extract, 5 nM:5 nM THC:CBD 1:1 plant extract, 100 nM SR1, 100 nM
412 SR2, and 10 nM methanandamide (mAEA). Unless otherwise specified in the figure legends or
413 text, all analyses were conducted 10 days after treatment withdrawal.
414
415 ***Generation and culture of breast cancer patient-derived organoids***
416 Patient-derived tumor samples were minced and digested as previously described (5),
417 using a pre-warmed digestion solution at 37 °C with constant shaking (150 rpm) for 2 hours. The
418 resulting suspension underwent sequential centrifugation at 500 × g. Cells were then carefully
419 resuspended in BME, and 20 µL drops were plated in pre-warmed 24-well plates. After the
420 Matrigel solidified, patient breast cancer (BC) organoid expansion medium was added. The
421 patient BC organoid expansion medium consisted of basal medium supplemented with 20%
422 homemade R-Spondin-1 conditioned medium, 1× B27 supplement, 1× N2 supplement, 10 mM
423 nicotinamide, 1.25 mM N-acetylcysteine, 10 nM Gastrin I, 100 ng/mL FGF10, 100 ng/mL Noggin,
424 50 ng/mL EGF, 5 nM Neuregulin 1, 5 µM Y-27632, 500 nM A83-01, 500 nM SB202190, and
425 Primocin. Organoids were passaged every 7-10 days, and the BC organoid expansion medium

426 was refreshed every two days. Cannabinoid treatments, dissolved in DMSO, were applied to
427 organoids for four days.
428
429 ***Cancer-Associated Fibroblast (CAF) extraction and culture***
430 Mammary gland tumors were harvested from PyMT mice at 6–8 weeks of age for CAF
431 isolation, as previously described (55, 56). Tumors were minced into small fragments and
432 digested in a prewarmed solution containing wash medium supplemented with 0.125 mg/mL
433 collagenase, 0.125 mg/mL dispase II, and 0.1 mg/mL DNase I. The suspension was incubated at
434 37 °C with constant shaking (120 rpm) for 2 hours. Following digestion, the cell suspension was
435 filtered through a 100 µm strainer and centrifuged at 500 x g. The pellet was resuspended in
436 selection medium (DMEM with 10% FBS, 1× Insulin-Transferrin-Selenium [ITS-G; Gibco,
437 41400045], and antibiotics) and incubated for 30 minutes to allow selective fibroblast adherence.
438 After incubation, the medium was replaced with CAF culture medium (DMEM supplemented with
439 10% FBS, 1× GlutaMAX, and antibiotics). CAF identity was confirmed by immunostaining: cells
440 were vimentin-positive (BD Biosciences, 5505013) and cytokeratin-negative (Abcam, ab7753).
441
442 ***Peripheral Blood Mononuclear Cell (PBMC) isolation***
443 Peripheral blood was collected via cardiac puncture from adult PyMT tumor-bearing mice
444 and transferred to EDTA-coated tubes to prevent coagulation. Samples were diluted 1:2 in HBSS
445 (Gibco, 14025092). PBMCs were isolated by density gradient centrifugation using Ficoll-Paque™
446 PLUS (VWR, 17-1440-02), at a ratio of 1 mL Ficoll per 3 mL of diluted blood. The blood was
447 carefully layered over Ficoll and centrifuged at 1600 rpm for 27 minutes at room temperature (no
448 brake, low acceleration). The PBMC layer was collected, transferred to a clean tube, and washed
449 three times with PBS supplemented with 1% FBS and antibiotics. Cells were counted and
450 cryopreserved for subsequent co-culture experiments.
451
452 ***Mammary tumor organoid–CAF co-culture***
453 PyMT-derived organoids were dissociated and co-seeded with primary CAFs at a 1:250
454 organoid-to-CAF ratio. CAFs were harvested from confluent cultures by incubation with 0.25%
455 trypsin and 0.1% EDTA (Corning, 25-053-CI) for 4 minutes at 37 °C. Detached cells were

456 collected in CAF medium, centrifuged at 600 x g, and kept on ice until use. Simultaneously,
457 organoids were harvested by mechanical disruption and washed twice by centrifugation at 500 x
458 g. For co-culture, 250 CAFs per organoid were added to the organoid suspension, followed by
459 centrifugation at 500 x g. The resulting pellet was gently resuspended in cold BME, and 20 µL
460 drops were plated into prewarmed 8-well chamber slides (Ibidi, 80841). After BME polymerization
461 at 37 °C, 200–300 µL of prewarmed breast cancer organoid expansion medium was added per
462 well. As experimental controls, organoids were cultured under identical conditions either alone
463 (without fibroblasts) or co-seeded with NIH/3T3 fibroblasts (ATCC CRL-1658™) using the same
464 protocol and ratio. Co-cultures and controls were evaluated at days 4 and 10 and subsequently
465 analyzed by immunofluorescence staining.
466
467 ***Co-culture of organoids with CAFs and PBMCs under shear stress in a flow-controlled***
468 ***bioreactor***
469 PyMT-derived breast cancer organoids were dissociated and co-seeded with primary
470 CAFs and autologous PBMCs (isolated from the same mouse). Organoids and CAFs were
471 seeded at a 1:250 ratio into µ-Slide III 3D Perfusion chambers (Ibidi, 80371). Following seeding,
472 chambers were incubated with breast cancer organoid expansion medium for 2 hours at 37 °C in
473 a humidified atmosphere with 5% CO_2 to promote cell attachment. Chambers were then
474 connected to a flow-controlled bioreactor system (57). The system included a peristaltic pump
475 (ISMATEC MCP, 78002-00) equipped with an 8-roller, 12-channel pump head (ISMATEC Type
476 IBM733A, 78002-36) and 1.52 mm PharMed BPT tubing (95723-36). µ-Slides were linked using
477 Ibidi elbow luer connectors (10802) and serial connectors (10830) to sterile silastic tubing (Dow
478 Corning 515-012). Organoid–CAF co-cultures were exposed to continuous capillary-level
479 physiological shear stress (2.6 dyn/cm²). PBMCs were introduced into the circulating medium,
480 allowing dynamic interaction with the organoid–CAF co-culture. The following experimental
481 conditions were established: (1) Organoids alone under static conditions; (2) Organoids under
482 flow (shear stress only); (3) Organoid–CAF co-culture under flow; (4) Organoid–CAF–PBMC co-
483 culture under flow; (5) Organoid–CAF–PBMC co-culture under flow, treated with either THC or
484 SR2. Cultures were analyzed at days 4 and 10 post-seeding.
485

486 ***Mammary gland orthotopic injection in vivo***

487 PyMT-derived organoids were treated with 10 nM THC for 4 days. After 10 days of
488 cannabinoid withdrawal in culture, organoids were resuspended in basal medium and centrifuged
489 at 500 × g. The resulting pellets were dissociated into single cells by incubating them for 20
490 minutes with TrypLE Select enzyme (Gibco, 12563011) at 37 °C with agitation. A total of 1×10^4
491 organoid-derived cells in 100 μL (50 μL cell suspension and 50 μL BME) were orthotopically
492 injected into the left inguinal mammary fat pad of 6-week-old PyMT wild-type sister mice, which
493 served as controls for the organoid-derived injections. Tumor formation was first observed at
494 week 3 post-inoculation for control (organoid-derived) tumors, and at week 5 for THC-pretreated
495 organoid-derived tumors. Mice were monitored three times a week for tumor growth, with tumor
496 length measured using external calipers. Tumor volume was calculated using the formula: $(4\pi/3)$
497 $\times$ $(\text{width}/2)^2 \times (\text{length}/2)^2$. When tumors reached a volume of 1000 mm^3, mice were euthanized,
498 and tumors were excised for evaluation. Tumors were fixed in 10% formalin and prepared for
499 immunohistochemistry analysis.

500

501 ***Analysis of metastasis in vivo***

502 PyMT-derived organoids were differentiated using 10 nM THC for 4 days and
503 subsequently cultured for an additional 14 days. Organoids were then minced and dissociated
504 into a single-cell suspension by incubating with TrypLE for 20 minutes. A total of 5×10^5 organoid-
505 derived cells per mouse were injected into the lateral tail vein of 6-week-old PyMT wild-type mice
506 to induce lung metastasis. Mice were euthanized four weeks post-injection. Lungs were then
507 excised, fixed, and prepared for both immunohistochemistry and immunofluorescence analyses.

508

509 ***Secondary organoid formation assay***

510 Organoids were collected and dissociated into single cells to assess their self-renewal
511 and organoid-forming potential. Samples were centrifuged at 500 × g, and the resulting pellets
512 were incubated with pre-warmed TrypLE for 20 minutes at 37°C. Gentle mechanical dissociation
513 was performed every 5 minutes. After dissociation, the samples were centrifuged again at 500 ×
514 g. Single cells were resuspended in BME at a density of 1×10^4 cells per 40 μL and seeded into
515 a 24-well plate. Following cell seeding, 650–1000 μL of BC organoid expansion medium was

516 added to each well. Cells were maintained at 37°C in a humidified incubator with 5% CO_2. The
517 medium was refreshed every two days, and organoid formation was evaluated after 10 days in
518 culture.
519
520 ***Cell cycle analysis***
521 After completing the differentiation protocol, organoid cultures were harvested and
522 centrifuged at 500 x g. Organoids were dissociated into single cells by incubating with TrypLE
523 Select at 37ºC for 20 minutes, with gentle pipetting every 5 minutes. The dissociated cells were
524 then fixed in ice-cold 70% ethanol for 30 minutes on ice. After fixation, the cells were centrifuged
525 at 800 x g. To degrade RNA and enable selective DNA staining, fixed cells were incubated with
526 100 µg/ml RNAse A (Sigma, R5503). Following RNA degradation, 400 µl of 50 µg/ml propidium
527 iodide (Sigma, P-4170) was added per $1x10^6$ cells. The samples were incubated on ice for 10
528 minutes and then analyzed using a FACScalibur flow cytometer (BD Biosciences).
529
530 ***Fluorescence-Activated Cell Sorting and subsequent organoid culture of PyMT:CB2R***
531 ***tumors***
532 Mammary gland tumors from PyMT:CB2R$^{+/+}$, and PyMT:CB2R$^{-/-}$ mice were excised and
533 processed for flow cytometry analysis. Tumors were minced and enzymatically digested in
534 digestion solution (wash medium supplemented with 0.125 mg/mL Collagenase and 0.125 mg/mL
535 Dispase II) for one hour at 37°C with shaking at 180 rpm. For single-cell suspension, the digested
536 tissue was centrifuged at 600 × g and filtered through a 100 µm cell strainer using 10 mL of
537 blocking buffer (wash buffer supplemented with 5 mM EDTA). The suspension was centrifuged
538 again at 600 × g, and erythrocytes were lysed by incubating the sample for 15 minutes at room
539 temperature. After a second filtration through a 100 µm cell strainer, the sample was centrifuged
540 again at 600 × g and resuspended in FACS buffer (PBS supplemented with 2% FBS, 0.01%
541 sodium azide, and antibiotics) at a concentration of 1×10^6 cells per 100 µL. Fc receptors were
542 blocked by incubating the cells with anti-CD16/32 antibody (1:100) for 20 minutes on ice. After
543 blocking, cells were washed and resuspended at the same concentration for staining with the
544 following antibodies: EpCAM-FITC (BioLegend, 118207) at a 1:200 dilution and CD49f-Alexa
545 Fluor™ 647 (BioLegend, 313610) at a 1:20 dilution. Cells were incubated with the antibody mix

546 for 20 minutes on ice in the dark. After staining, samples were centrifuged at 1000 × g at 4°C and
547 resuspended in FACS buffer at a concentration of 1×10^6 cells in 100 μL, and stained with 7-AAD
548 (BioLegend, 420404) as a viability marker at a 1:50 dilution. Cells were sorted using a FACSAria
549 III cell sorter (BD Biosciences) into four distinct populations based on differential expression of
550 CD49f and EpCAM. FlowJo™ software was used for data analysis. Each population was collected
551 separately and used to initiate organoid cultures. Sorted cells were seeded at a density of 1×10^4
552 cells per well in 40 μL of BME in a pre-warmed 24-well plate. After matrix polymerization, 650–
553 1000 μL of BC organoid expansion medium was added to each well. Cultures were maintained
554 at 37°C with 5% CO_2, with unsorted cells serving as the control for organoid formation. Medium
555 was refreshed every 48 hours. Organoid formation was evaluated after 10 days in culture to
556 assess the growth potential of each sorted population.
557
558 ***Apoptosis assay by flow cytometry***
559 Organoid cultures were harvested and transferred to a tube for dissociation into single
560 cells. Pre-warmed TrypLE Select was used for cell dissociation, with incubation for 20 minutes at
561 37ºC. After digestion, cells were centrifuged at 500 x g. Apoptosis analysis was performed using
562 the Dead Cell Apoptosis Kit with Annexin V for Flow Cytometry (Invitrogen, V13445), according
563 to the manufacturer's instructions. Briefly, cells were stained with a 1:100 dilution of Annexin V-
564 Alexa Fluor™ 488 and 0.2 μg/ml propidium iodide (PI) solution in annexin-binding buffer. The
565 samples were incubated at room temperature for 15 minutes in the dark. Following incubation,
566 samples were analyzed using a FACScalibur flow cytometer.
567
568 ***Cell viability assay***
569 Organoids and primary tumor cells derived from PyMT mice were assessed for viability
570 based on intracellular ATP content using the CellTiter-Glo® 3D Cell Viability Assay (Promega,
571 G9682), following the manufacturer's instructions. Briefly, cells were lysed with the CellTiter-Glo
572 3D reagent, and luminescence was measured using an IVIS Spectrum system (PerkinElmer).
573 Background signals from the medium were subtracted, and relative luminescence units (RLU)
574 were normalized to control conditions.
575

576 ***Cellular migration analysis from patient-derived samples***

577 To investigate cellular migration traits in detail, we employed the HoloMonitor® M4, an
578 automated live-cell imaging cytometer that performs time-lapse analysis. This system allows for
579 the imaging and quantification of unstained, living cells directly within their culture vessels inside
580 the incubator, enabling real-time monitoring of various morphological and migratory parameters.
581 Based on digital holographic microscopy, the HoloMonitor measures phase shifts in light as it
582 passes through cells, which the software then uses to reconstruct high-resolution topographic
583 images. For our experiments, we used ibidi® plastic 24-well plates fitted with HoloLid™ lids—
584 specifically designed to reduce image artifacts caused by surface vibrations and condensation.
585 We quantified the following parameters: Cell area (μm²), the surface area occupied by each cell;
586 Irregularity, the degree to which a cell's outline deviates from a perfect circle; Migration (μm), the
587 shortest linear distance between a cell's initial and final positions; Motility (μm), the total path
588 length traveled by a cell; Motility speed (μm/h), the motility distance divided by the observation
589 time. Statistical analyses were performed using R software (version 4.5.0, RCore2013). For each
590 parameter, we calculated the mean ± standard error of the mean (SEM). A generalized linear
591 model (glm) (58) was fitted to assess the impact of experimental conditions, time and their
592 interaction on each variable. Variables were log transformed to verify assumptions of normality
593 and homoscedasticity.

594

595 ***Cytokine profiling from co-culture conditioned media***

596 Cytokine secretion profiles from co-culture conditions were analyzed using the Proteome
597 Profiler Mouse Cytokine Array Kit, Panel A (R&D Systems, ARY006), according to the
598 manufacturer's protocol. Briefly, 1 mL of conditioned media was collected from cell cultures,
599 centrifuged at 500 x g to remove cellular debris, and the supernatants were transferred to fresh
600 tubes and stored at -20°C until processing. Array membranes were blocked and incubated with
601 the Detection Antibody Cocktail. The antibody-sample mixture was applied to the membranes,
602 which were incubated overnight at 4°C. The following day, membranes were washed, incubated
603 with Streptavidin-HRP for 30 minutes, and developed using a chemiluminescent reagent. Signals
604 were detected using the ChemiDoc XRS+ Imaging System (BioRad). Cytokine spot intensities
605 were quantified using Fiji (ImageJ) and normalized to positive controls.

606 ***Immunofluorescence***

607 For immunofluorescence analysis, organoids were seeded into 8-well chamber slides
608 with removable wells (Nunc™ Lab-Tek™ II Chamber Slide™ System 154534) during the final
609 week of the culture period. Cells were briefly rinsed with phosphate-buffered saline (PBS) prior to
610 fixation. Organoids were fixed with 10% formalin for 1 hour at room temperature (RT).
611 Permeabilization was performed using 3% Triton X-100 (Sigma, T9284) in PBS for 20 minutes,
612 followed by three washes with 0.1% Triton X-100 in PBS. Blocking was carried out with blocking
613 solution (PBS + 0.1% Triton X-100 + 2% bovine serum albumin (BSA) [Sigma, A6003]) for 2.5
614 hours at RT. Primary antibodies were diluted in the blocking solution and added to the samples,
615 which were then incubated overnight at 4°C. After incubation, samples were washed with PBS,
616 and secondary antibodies were applied at a 1:500 dilution in the blocking solution. Incubation with
617 secondary antibodies was done at RT for 1.5 hours in dark conditions. After secondary antibody
618 incubation, samples were washed twice with PBS. For nuclear staining, DAPI was diluted 1:1000
619 in PBS and added to each well for a 10-minute incubation. After staining, the cells were mounted
620 using Mowiol 4-88 (Calbiochem, 475904) as the mounting medium. The primary antibodies used
621 for IF staining and their respective dilutions are as follows: **Cytokeratin 14** (rabbit monoclonal
622 EPR17350, Abcam, ab181595) at 1:100 dilution. **Cytokeratin 8/18** (mouse monoclonal TROMA-
623 I, DSHB, ab_531826) at 1:100 dilution. **Ki67** (mouse monoclonal B56, BD Biosciences, 550609)
624 at 1:400 dilution. **E-cadherin** (rabbit monoclonal 24E10, Cell Signaling, 3195S) at 1:500 dilution.
625 **Snail** (mouse monoclonal L70G2, Cell Signaling, 3895) at 1:250 dilution. **CD49f-Alexa Fluor™**
626 **647** (rat monoclonal GoH3, BioLegend, 313610) at 1:100 dilution. **EpCAM** (rat monoclonal G8.8,
627 BioLegend, 118207) at 1:200 dilution. **SOX10** (rabbit monoclonal EPR4007, Abcam, ab155279)
628 at 1:250 dilution. **CD24-Alexa Fluor™ 488** (rat monoclonal M1/69, BioLegend, 101816) at 1:800
629 dilution. **H3K9me3** (rabbit polyclonal, Abcam, ab8898) at 1:400 dilution. **H3K4me3** (rabbit
630 monoclonal EPR20551-225, Abcam, ab213224) at 1:100 dilution. **H3K27me3** (mouse
631 monoclonal, Abcam ab6002) at 1:200 dilution. **Phalloidin-Rhodamine** (Invitrogen R415) at 1:200
632 dilution. Samples were examined using a TCS SP8 laser scanning confocal microscope (Leica).
633 Image acquisition was performed in a sequential scanning mode by optimizing lasers and spectral
634 detectors for each specific fluorescent dye. Z-stacks were obtained by 2.5 µm z-steps, a 20X oil
635 immersion objective and a 1024x1024 scanning resolution. Image processing and analyses were

636 performed using Fiji (ImageJ). 3D projections were generated using the brightest point projection
637 method.
638
639 ***Immunohistochemistry***
640 Mammary gland and lung tissue samples were fixed in 10% formalin, paraffin-embedded,
641 and sectioned at 4 µm. The sections were mounted on Superfrost Plus slides and dried overnight.
642 Slides were stained with hematoxylin and eosin (H&E) or subjected to immunohistochemical
643 analysis. Antigen retrieval was performed, followed by blocking of endogenous peroxidase activity
644 using 3% hydrogen peroxide. The slides were then incubated with primary antibodies specific for
645 the following targets: **Cytokeratin 14** (rabbit polyclonal AF64, Covance, PRB-155P), **Cytokeratin**
646 **8/18** (rabbit monoclonal, Dako, IR094), **SOX9** (rabbit polyclonal, Millipore, AB5535), **SOX10** (goat
647 polyclonal N-20, Santa Cruz, c-17342), **Ki-67** (rabbit monoclonal D3B5, Cell Signaling, 12202),
648 and **Estrogen Receptor alpha** (mouse monoclonal CRET94D/H9). Secondary antibodies,
649 conjugated with horseradish peroxidase (OmniRabbit, Ventana, Roche), were applied, and the
650 immunohistochemical reaction was developed using 3,3'-diaminobenzidine tetrahydrochloride
651 (DAB) as the chromogen (Chromomap DAB, Ventana, Roche or DAB solution, Dako). Nuclei
652 were counterstained with Carazzi's hematoxylin. Finally, the slides were dehydrated, cleared, and
653 mounted with a permanent mounting medium for microscopic evaluation.
654
655 ***RNA extraction and analysis of mRNA levels***
656 RNA was extracted using NucleoZOL™ (Takara Bio) following the manufacturer's
657 instructions. Reverse transcription (RT) was performed from 1 µg of RNA using the Transcriptor
658 First Strand cDNA Synthesis Kit (Roche, 04379012001) with random hexamer primers.
659 Quantitative real-time PCR was then conducted using the PowerUp™ SYBR™ Green Master Mix
660 (Applied Biosystems, A25742), following the manufacturer's guidelines, using 50 ng of cDNA per
661 well in a 384-well plate. Data were acquired with a QuantStudio™ 12K Flex system (Applied
662 Biosystems). The following primers were used (5′−3′ sequence; F: Forward, R: Reverse): **Krt5**.
663 F: TCC TGT TGA ACG CCG CTG AC; R: CGG AAG GAC ACA CTG GAC TGG; **Krt14**. F: CAG
664 CCC CTA CTT CAA GAC CA; R: GTC GAT CTG CAG GAG GAC AT; **Krt8**. F: GGA CAT CGA
665 GAT CAC CAC CT; R: TGA AGC CAG GGC TAG TGA GT; **Krt18**. F: CAA GTC TGC CGA AAT

666 CAG GGA C; R: TCC AAG TTG ATG TTC TGG TTT T; **Cdh1**. F: AGG AAA TGC ACC CCT CCA
667 AT; R: AAT CGG CCA GCA TTT TCT G; **Cdh2**. F: GCC ATC ATC GCT ATC CTT CT; R: CCG
668 TTT CAT CCA TAC CAC AAA; **Vimentin**. F: CCA ACC TTT TCT TCC CTG AAC; R: TTG AGT
669 GGG TGT CAA CCA GA; **Sox10**. F: ATC AGC CAC GAG GTA ATG TCC AAC; R: ACT GCC
670 CAG CCC GTA GCC; **EpCAM**. F: GAT TCT GCA CGT GAG ACC TG; R: GAT ACC AAG TCA
671 AAC CGA GAA CTT.
672
673 ***RNA sequencing***
674 RNA was extracted using Nucleozol™ following the manufacturer's instructions. RNA-
675 seq sample preparation and initial data analysis were carried out by Novogene. In brief,
676 transcriptome libraries were generated from high-quality RNA samples (triplicates), which were
677 verified using the Agilent Bioanalyzer 2100. Messenger RNA was isolated using poly-T oligo-
678 attached magnetic beads, then fragmented prior to cDNA synthesis. Both non-stranded and
679 strand-specific libraries were prepared according to standard Illumina protocols. Library quality
680 was assessed using Qubit, qPCR, and Bioanalyzer analysis. Sequencing was performed on an
681 Illumina platform utilizing sequencing-by-synthesis technology to generate high-throughput reads.
682 Bioinformatic analysis began with quality control of raw reads using FastQC. Clean reads were
683 mapped to the reference genome with HISAT2. Differential expression was analyzed using
684 DESeq2, applying a threshold of adjusted $p \leq 0.05$ and $|\log2FC| \geq 1$. Functional enrichment was
685 performed using the clusterProfiler R package, with analysis across GO, KEGG, Reactome, DO,
686 and DisGeNET databases.
687
688 ***Statistical analysis***
689 All experiments were performed with at least three independent biological replicates.
690 Data are presented as mean ± SEM, and p-values ≤ 0.05 were considered statistically significant.
691 For comparisons between two independent groups, a two-tailed Student's t-test was used.
692 Correlations between two variables were calculated using Pearson's r. For multi-group
693 comparisons, data were analyzed using one-way ANOVA with post-hoc Tukey's multiple
694 comparison test, or two-way ANOVA when appropriate. Statistical analyses were performed using
695 GraphPad Prism software (version 10.1.2).

696 ***Data availability***

697 RNAseq data has been deposited in the SRA repository under BioProject accession
698 number PRJNA1276513.

699

700 **Acknowledgements:** We thank the CNIO Histopathology and Genomics Units, UCM Confocal
701 Unit and UCM Animal Facility for their technical support. We are indebted to the members of the
702 Cannabinoid Signaling group (UCM), Eva Resel for administrative support, and to our former
703 undergraduate and master students, with special mention to Marc Pinto, Manuel Luque, and
704 Paula Gijón. We would like to express our thanks to Novogene Europe for their technical and
705 customer support, with special appreciation to Metehan Cifdaloz, Paula Yagüe, and Haozhen Su.
706 We are also extremely grateful to the Hospital *La Paz*, particularly to the Gynecology and
707 Histopathology Units, for their constructive participation in this work and very specially, to the
708 patients enrolled in this research study. This work has been in part financed by benefactors,
709 through multiple donations to *Asociación Española contra el Cáncer* (AECC). We are extremely
710 thankful to all our anonymous donors. The work has been funded by the Spanish Ministry of
711 Science, Innovation and Universities, supported with European Regional Development funds:
712 **CNS2022-135364** and **PID2022-136508OA-I00**, and the Complutense University, through the
713 project **PR3/23-30841** to MS-R. MS-R was also supported by AECC (**INVES18005SALA**) and a
714 *Ramón y Cajal* contract from the Ministry of Science, Innovation and Universities (**RYC2020-**
715 **028929-I**). NGM-I was supported by AECC (**PRDMA19003GARC**) and Fulbright fellowship
716 (**PS00380044**). ERE and MB were supported by National Institutes of Health (NIH) Research
717 Project Grant **R01 HL 161069**.

718

719 **Author contributions:** NGM-I conducted most of the cellular and *in vivo* experiments, with
720 assistance from GP-G, MR-H, CQ-G, EM-Z, and MS-R. The Flow Cytometry and Confocal
721 Imaging Unit at UCM (LMA-C and CH) collaborated on confocal imaging analyses and flow
722 cytometry experiments. The Histopathology Unit at CNIO performed IHC experiments and
723 provided professional histopathological analyses of the samples when needed (EC). MM-R and
724 AZ-C contributed to RNA sequencing experiments, with support from NGM-I, CQ-G, and MS-R.
725 AP-P collaborated with EM-Z and NGM-I to perform the R analysis of patient-derived data. LF-A

726 assisted in preparing the necessary documents and protocols for patient enrollment at the
727 hospital, recruited patients, and offered clinical advice. CS, MB-C and ERE provided guidance,
728 materials and/or resources. MB-C and ERE directly contributed to the optimization and execution
729 of dynamic cell co-culture experiments alongside NGM-I. MS-R and NGM-I supervised the project
730 design, data evaluation and analysis. MS-R conceived the study, managed the teamwork and
731 wrote the manuscript with contributions from the primary authors.
732
733 **Competing interest:** The authors declare no competing financial interests.
734
735 **Ethical approvals:** All animal procedures were conducted at the Animal Facility of the Faculty of
736 Biology, Complutense University of Madrid (UCM). The experimental protocols involving animals
737 adhered to local regulations (RD53/2013 and ECC/566/2015) and were approved by the relevant
738 Regulatory Agencies, including Complutense University and the Community of Madrid. All authors
739 involved in animal experimentation hold the necessary accreditation (categories C and D) granted
740 by the Competent Authority: CAP-T-0771-15, CAM Animal Welfare Committee on Animal
741 Experimentation. Regarding patient protection, all procedures followed the guidelines of Hospital
742 La Paz, local regulations, and the Declaration of Helsinki, as well as the Guidelines for Good
743 Clinical Practice (GCP) established by the International Conference on Harmonization (ICH E6).
744 The protocols for sample collection, processing, and any additional materials provided to the
745 patients (e.g., Patient Information Sheets and the Informed Consent Document) were approved
746 by the Clinical Research Ethics Committee of *Hospital La Paz*, in full compliance with national
747 legislation.

748 **References**

749 1. Hanahan D. Hallmarks of Cancer: New Dimensions. Cancer Discov. 2022;12(1):31-46.
750
751 2. de The H. Differentiation therapy revisited. Nat Rev Cancer. 2018;18(2):117-27.
752
753 3. Sole R, Aguade-Gorgorio G. The ecology of cancer differentiation therapy. J Theor Biol.
754 2021;511:110552.
755
756 4. Kim SI, Sohn J, Koo JS, Park SH, Park HS, Park BW. Molecular subtypes and tumor
757 response to neoadjuvant chemotherapy in patients with locally advanced breast cancer.
758 Oncology. 2010;79(5-6):324-30.
759
760 5. Martinez-Illescas NG, Leal S, Gonzalez P, Grana-Castro O, Munoz-Oliveira JJ, Cortes-
761 Pena A, et al. miR-203 drives breast cancer cell differentiation. Breast Cancer Res.
762 2023;25(1):91.
763
764 6. Salazar-Roa M, Trakala M, Alvarez-Fernandez M, Valdes-Mora F, Zhong C, Munoz J, et
765 al. Transient exposure to miR-203 enhances the differentiation capacity of established pluripotent
766 stem cells. EMBO J. 2020;39(16):e104324.
767
768 7. Dreesen O, Brivanlou AH. Signaling pathways in cancer and embryonic stem cells. Stem
769 Cell Rev. 2007;3(1):7-17.
770
771 8. Hanahan D, Weinberg RA. The hallmarks of cancer. Cell. 2000;100(1):57-70.
772
773 9. Batlle E, Clevers H. Cancer stem cells revisited. Nat Med. 2017;23(10):1124-34.
774 10. Takebe N, Harris PJ, Warren RQ, Ivy SP. Targeting cancer stem cells by inhibiting Wnt,
775 Notch, and Hedgehog pathways. Nat Rev Clin Oncol. 2011;8(2):97-106.
776
777 11. Takebe N, Ivy SP. Controversies in cancer stem cells: targeting embryonic signaling
778 pathways. Clin Cancer Res. 2010;16(12):3106-12.
779
780 12. Liu J, Xiao Q, Xiao J, Niu C, Li Y, Zhang X, et al. Wnt/beta-catenin signalling: function,
781 biological mechanisms, and therapeutic opportunities. Signal Transduct Target Ther. 2022;7(1):3.
782
783 13. Nwabo Kamdje AH, Takam Kamga P, Tagne Simo R, Vecchio L, Seke Etet PF, Muller
784 JM, et al. Developmental pathways associated with cancer metastasis: Notch, Wnt, and
785 Hedgehog. Cancer Biol Med. 2017;14(2):109-20.

786

14. Bolos V, Grego-Bessa J, de la Pompa JL. Notch signaling in development and cancer. Endocr Rev. 2007;28(3):339-63.

15. Huang JJ, Blobe GC. Dichotomous roles of TGF-beta in human cancer. Biochem Soc Trans. 2016;44(5):1441-54.

16. Larue L, Bellacosa A. Epithelial-mesenchymal transition in development and cancer: role of phosphatidylinositol 3' kinase/AKT pathways. Oncogene. 2005;24(50):7443-54.

17. Rah B, Rather RA, Bhat GR, Baba AB, Mushtaq I, Farooq M, et al. JAK/STAT Signaling: Molecular Targets, Therapeutic Opportunities, and Limitations of Targeted Inhibitions in Solid Malignancies. Front Pharmacol. 2022;13:821344.

18. Hinz B, Ramer R. Cannabinoids as anticancer drugs: current status of preclinical research. Br J Cancer. 2022;127(1):1-13.

19. Ligresti A, De Petrocellis L, Di Marzo V. From Phytocannabinoids to Cannabinoid Receptors and Endocannabinoids: Pleiotropic Physiological and Pathological Roles Through Complex Pharmacology. Physiol Rev. 2016;96(4):1593-659.

20. Maccarrone M. Missing Pieces to the Endocannabinoid Puzzle. Trends Mol Med. 2020;26(3):263-72.

21. Ramer R, Schwarz R, Hinz B. Modulation of the Endocannabinoid System as a Potential Anticancer Strategy. Front Pharmacol. 2019;10:430.

22. Velasco G, Sanchez C, Guzman M. Towards the use of cannabinoids as antitumour agents. Nat Rev Cancer. 2012;12(6):436-44.

23. Gaoni Y, Mechoulam R. Isolation, Structure, and Partial Synthesis of an Active Constituent of Hashish. J Am Chem Soc. 1964;86(8):1646-+.

24. Oesch S, Gertsch J. Cannabinoid receptor ligands as potential anticancer agents--high hopes for new therapies? J Pharm Pharmacol. 2009;61(7):839-53.

25. Guzman M, Duarte MJ, Blazquez C, Ravina J, Rosa MC, Galve-Roperh I, et al. A pilot clinical study of Delta9-tetrahydrocannabinol in patients with recurrent glioblastoma multiforme. Br J Cancer. 2006;95(2):197-203.

826 26. Dumitru CA, Sandalcioglu IE, Karsak M. Cannabinoids in Glioblastoma Therapy: New
827 Applications for Old Drugs. Front Mol Neurosci. 2018;11:159.
828
829 27. Twelves C, Sabel M, Checketts D, Miller S, Tayo B, Jove M, et al. A phase 1b
830 randomised, placebo-controlled trial of nabiximols cannabinoid oromucosal spray with
831 temozolomide in patients with recurrent glioblastoma. Br J Cancer. 2021;124(8):1379-87.
832
833 28. Bhaskaran D, Savage J, Patel A, Collinson F, Mant R, Boele F, et al. A randomised phase
834 II trial of temozolomide with or without cannabinoids in patients with recurrent glioblastoma
835 (ARISTOCRAT): protocol for a multi-centre, double-blind, placebo-controlled trial. BMC Cancer.
836 2024;24(1):83.
837
838 29. Willyard C. Cancer therapy: an evolved approach. Nature. 2016;532(7598):166-8.
839
840 30. Perez-Gomez E, Andradas C, Blasco-Benito S, Caffarel MM, Garcia-Taboada E, Villa-
841 Morales M, et al. Role of cannabinoid receptor CB2 in HER2 pro-oncogenic signaling in breast
842 cancer. J Natl Cancer Inst. 2015;107(6):djv077.
843
844 31. Raina K, Dey C, Thool M, Sudhagar S, Thummer RP. An Insight into the Role of UTF1 in
845 Development, Stem Cells, and Cancer. Stem Cell Rev Rep. 2021;17(4):1280-93.
846
847 32. Jia J, Zheng X, Hu G, Cui K, Zhang J, Zhang A, et al. Regulation of pluripotency and self-
848 renewal of ESCs through epigenetic-threshold modulation and mRNA pruning. Cell.
849 2012;151(3):576-89.
850
851 33. Gatenby RA, Silva AS, Gillies RJ, Frieden BR. Adaptive therapy. Cancer Res.
852 2009;69(11):4894-903.
853
854 34. Early Breast Cancer Trialists' Collaborative G, Davies C, Godwin J, Gray R, Clarke M,
855 Cutter D, et al. Relevance of breast cancer hormone receptors and other factors to the efficacy
856 of adjuvant tamoxifen: patient-level meta-analysis of randomised trials. Lancet.
857 2011;378(9793):771-84.
858
859 35. Pierce GB, Wallace C. Differentiation of malignant to benign cells. Cancer Res.
860 1971;31(2):127-34.
861
862 36. Huang ME, Ye YC, Chen SR, Chai JR, Lu JX, Zhoa L, et al. Use of all-trans retinoic acid
863 in the treatment of acute promyelocytic leukemia. Blood. 1988;72(2):567-72.
864

865 37. Cruz FD, Matushansky I. Solid tumor differentiation therapy - is it possible? Oncotarget.
866 2012;3(5):559-67.
867
868 38. Pagano C, Navarra G, Coppola L, Avilia G, Bifulco M, Laezza C. Cannabinoids:
869 Therapeutic Use in Clinical Practice. Int J Mol Sci. 2022;23(6).
870
871 39. Galve-Roperh I, Sanchez C, Cortes ML, Gomez del Pulgar T, Izquierdo M, Guzman M.
872 Anti-tumoral action of cannabinoids: involvement of sustained ceramide accumulation and
873 extracellular signal-regulated kinase activation. Nat Med. 2000;6(3):313-9.
874
875 40. Pyszniak M, Tabarkiewicz J, Luszczki JJ. Endocannabinoid system as a regulator of
876 tumor cell malignancy - biological pathways and clinical significance. Onco Targets Ther.
877 2016;9:4323-36.
878
879 41. Liu WM, Scott KA, Shamash J, Joel S, Powles TB. Enhancing the in vitro cytotoxic activity
880 of Delta9-tetrahydrocannabinol in leukemic cells through a combinatorial approach. Leuk
881 Lymphoma. 2008;49(9):1800-9.
882
883 42. Kampa-Schittenhelm KM, Haverkamp T, Bonin M, Tsintari V, Buhring HJ, Haeusser L, et
884 al. Epigenetic activation of O-linked beta-N-acetylglucosamine transferase overrides the
885 differentiation blockage in acute leukemia. EBioMedicine. 2020;54:102678.
886
887 43. Sido JM, Yang X, Nagarkatti PS, Nagarkatti M. Delta9-Tetrahydrocannabinol-mediated
888 epigenetic modifications elicit myeloid-derived suppressor cell activation via STAT3/S100A8. J
889 Leukoc Biol. 2015;97(4):677-88.
890
891 44. Tomko AM, Whynot EG, Ellis LD, Dupre DJ. Anti-Cancer Potential of Cannabinoids,
892 Terpenes, and Flavonoids Present in Cannabis. Cancers (Basel). 2020;12(7).
893 45. Mangal N, Erridge S, Habib N, Sadanandam A, Reebye V, Sodergren MH. Cannabinoids
894 in the landscape of cancer. J Cancer Res Clin Oncol. 2021;147(9):2507-34.
895
896 46. Howlett AC, Barth F, Bonner TI, Cabral G, Casellas P, Devane WA, et al. International
897 Union of Pharmacology. XXVII. Classification of cannabinoid receptors. Pharmacol Rev.
898 2002;54(2):161-202.
899
900 47. Begbie J, Doherty P, Graham A. Cannabinoid receptor, CB1, expression follows neuronal
901 differentiation in the early chick embryo. J Anat. 2004;205(3):213-8.
902

903 48. Mulder J, Aguado T, Keimpema E, Barabas K, Ballester Rosado CJ, Nguyen L, et al.
904 Endocannabinoid signaling controls pyramidal cell specification and long-range axon patterning.
905 Proc Natl Acad Sci U S A. 2008;105(25):8760-5.
906
907 49. Wang X, Dow-Edwards D, Keller E, Hurd YL. Preferential limbic expression of the
908 cannabinoid receptor mRNA in the human fetal brain. Neuroscience. 2003;118(3):681-94.
909
910 50. Pagano C, Navarra G, Coppola L, Bifulco M, Laezza C. Molecular Mechanism of
911 Cannabinoids in Cancer Progression. Int J Mol Sci. 2021;22(7).
912
913 51. Okuda A, Fukushima A, Nishimoto M, Orimo A, Yamagishi T, Nabeshima Y, et al. UTF1,
914 a novel transcriptional coactivator expressed in pluripotent embryonic stem cells and extra-
915 embryonic cells. EMBO J. 1998;17(7):2019-32.
916
917 52. Lou Y, Jin S, Hong X, Hong Z, Xu C. Expression and clinical significance of
918 undifferentiated embryonic cell transcription factor 1 in breast cancer. Transl Cancer Res.
919 2023;12(1):150-62.
920
921 53. Wu XL, Zheng PS. Undifferentiated embryonic cell transcription factor-1 (UTF1) inhibits
922 the growth of cervical cancer cells by transactivating p27Kip1. Carcinogenesis. 2013;34(7):1660-
923 8.
924
925 54. Smoum R, Grether U, Karsak M, Vernall AJ, Park F, Hillard CJ, et al. Editorial:
926 Therapeutic potential of the cannabinoid CB2 receptor. Front Pharmacol. 2022;13:1039564.
927
928 55. Primac I, Maquoi E, Blacher S, Heljasvaara R, Van Deun J, Smeland HY, et al. Stromal
929 integrin alpha11 regulates PDGFR-beta signaling and promotes breast cancer progression. J Clin
930 Invest. 2019;129(11):4609-28.
931
932 56. Sharon Y, Alon L, Glanz S, Servais C, Erez N. Isolation of normal and cancer-associated
933 fibroblasts from fresh tissues by Fluorescence Activated Cell Sorting (FACS). J Vis Exp.
934 2013(71):e4425.
935
936 57. Salazar-Martin AG, Kalluri AS, Villanueva MA, Hughes TK, Wadsworth MH, 2nd, Dao TT,
937 et al. Single-Cell RNA Sequencing Reveals That Adaptation of Human Aortic Endothelial Cells to
938 Antiproliferative Therapies Is Modulated by Flow-Induced Shear Stress. Arterioscler Thromb Vasc
939 Biol. 2023;43(12):2265-81.
940

58. Bolker BM, Brooks ME, Clark CJ, Geange SW, Poulsen JR, Stevens MH, et al. Generalized linear mixed models: a practical guide for ecology and evolution. Trends Ecol Evol. 2009;24(3):127-35.

945 **Figure legends**

946

947 **Figure 1. A brief nanomolar THC exposure induces a long-term basal-to-luminal**
948 **morphological and molecular switch in MMTV-PyMT mammary tumor organoids. A**,
949 Schematic of the experimental design. PyMT-derived tumor organoids were treated with vehicle
950 (DMSO) or 10 nM THC for 4 days, followed by extended culture. Analyses were performed at 1-,
951 2-, and 3-weeks post-treatment. **B**, Representative brightfield images of control and THC-treated
952 organoids at 2 weeks. *n*=6 independent experiments. Scale bar, 100 µm. **C**, Confocal images of
953 organoids stained for CD24 (green) and CD49f (red) -cell surface markers of mammary gland
954 precursor- at 1, 2, and 3 weeks, showing temporal changes in morphology and marker expression
955 after THC exposure. DAPI (blue) stains nuclei. Upper panels show 3D stacks; lower panels show
956 representative single slices. *n*=3 independent experiments. Scale bar, 100 µm. **D**, Quantification
957 of organoids classified as granular (basal), mid (intermediate), or cystic (luminal/rounded) over
958 time. *n*=3 independent experiments; *p<0.05, **p<0.01, ***p<0.001 vs. control (granular);
959 #p=0.014 vs. control (cystic) (Two-way ANOVA). **E**, Quantification of organoid size (µm) at
960 endpoint. *n*=3 independent experiments; 80–100 organoids per condition; ****p<0.0001 (unpaired
961 Student's t-test). **F**, Confocal images of organoids at 2 weeks stained for CK14 (green; basal
962 marker) and CK8/18 (red; luminal marker). Left: 3D stacks; middle: single slices; right: merged
963 with brightfield. DAPI (blue) stains nuclei. *n*=4 independent experiments. Scale bar, 100 µm. **G**,
964 qPCR analysis of cytokeratin genes (CK14/5 and CK8/18, denoting a basal-like and luminal-like
965 phenotypes, respectively) at endpoint, normalized to GAPDH. *n*=3 independent experiments;
966 *p<0.05, **p<0.01 (unpaired Student's t-test).

967

968 **Figure 2. Brief exposure to nanomolar THC prevents collective migration, promotes**
969 **mesenchymal-to-epithelial transition, and reduces self-renewal in mammary tumor**
970 **organoids. A,** Representative confocal images of basal organoids showing collective migration
971 in control cultures. Organoids are stained for E-CAD (green) and SNAIL (red) (left) -as EMT
972 markers- or CK14 (green) and CK8/18 (red) (right). Note the cellular projections extending from
973 the organoid edges and attaching to the substrate. The inset highlights preserved E-CAD staining
974 in migrating areas, indicating cohesive cell movement. DAPI (blue) stains nuclei. *n*=3 independent

975 experiments. Scale bar, 100 μm. **B**, Quantification of the two-dimensional area (μm²) of collective-
976 migratory projections in control vs. THC-treated cultures at 2 weeks. *n*=3 independent
977 experiments; 25–30 organoids per condition; ***p<0.001 (unpaired Student's t-test).
978 Representative brightfield images (right) illustrate measured areas. Scale bar, 100 μm. **C**, qPCR
979 analysis of EMT-related genes at day 14. mRNA levels were normalized to GAPDH. *n*=3
980 independent experiments; *p<0.05 (unpaired Student's t-test). **D**, Time-course comparison of
981 organoids displaying collective migration in control vs. THC-treated conditions. *n*=3 independent
982 experiments; *p<0.05 (unpaired Student's t-test). **E**, Quantification of secondary organoid
983 formation from single-cell dissociation at 21 days, indicating self-renewal capacity. *n*=6
984 independent experiments; ***p<0.001 (unpaired Student's t-test). **F**, Confocal images of
985 organoids stained for CD49f (red), EpCAM (green), and SOX10 (white; stemness marker) after
986 treatment with vehicle or 10 nM THC and analyzed at 2 weeks. DAPI (blue) stains nuclei. Merged
987 images with brightfield are shown on the right. *n*=4 independent experiments. Scale bar, 100 μm.
988 **G**, qPCR analysis of stemness and differentiation markers (Sox10, EpCAM) at day 14. Data
989 normalized to GAPDH. *n*=3 independent experiments; *p<0.05 (unpaired Student's t-test).
990
991 **Figure 3. *In vivo* functional evidence of THC-induced tumor cell differentiation.**
992 **A**, Schematic of the experimental design. MMTV-PyMT-derived organoids were treated with
993 vehicle or THC (10 nM) for 4 days, cultured drug-free for 10 days, and orthotopically injected into
994 PyMT wild-type littermates. Mice (*n*=8 vehicle, *n*=8 THC) were monitored for 100 days to assess
995 tumor onset and growth. **B**, Brightfield and immunofluorescence images of organoids treated as
996 indicated and analyzed before injection. Organoids showed expected expression of basal (CK14;
997 green) or luminal (CK8/18; red) markers. DAPI (blue) stains nuclei. Scale bar, 100 μm. **C**, Kaplan-
998 Meier plot showing tumor onset (% of mice with tumors) over time. **p<0.01 (Two-way ANOVA).
999 **D**, Quantification of tumor volume (mm³) in both groups. ****p<0.0001 (Two-way ANOVA). **E**,
1000 Histopathological classification of tumors at endpoint (100 days): expanded/focal infiltrating
1001 neoplasia, local neoplasia, hyperplasia, or no tumor cells. **p<0.01 (Two-way ANOVA). Right:
1002 H&E-stained images of representative infiltrating neoplasia (control) and localized hyperplasia
1003 (THC). Scale bar, 500 μm. **F**, Schematic of metastasis assay. Organoids were treated with vehicle
1004 or THC (10 nM) for 4 days, cultured for 2 additional weeks, and injected via tail vein into PyMT

1005 wild-type mice. Lung metastases were assessed one-month post-injection (*n*=9 vehicle, *n*=7
1006 THC). **G**, Distribution of micro- and macro-metastases in lung tissue per condition. *p<0.05 (Two-
1007 way ANOVA). Right: H&E-stained images of representative lung metastases. Scale bar, 500 µm.
1008 **H**, Quantification of micro-metastases per animal. Each dot represents one mouse. **p<0.01
1009 (Two-way ANOVA). **I**, Immunofluorescence of lung sections stained for CK14, indicating micro-
1010 metastases. DAPI (blue) stains nuclei. Scale bar, 500 µm.
1011
1012 **Figure 4. SR2, but not SR1, mimics THC in promoting a basal-to-luminal switch, blocking**
1013 **collective migration, and reducing self-renewal in mammary tumor organoids.**
1014 **A**, Representative brightfield images of organoids treated for 4 days with vehicle, THC (10 nM),
1015 SR1 (100 nM), or SR2 (100 nM), and analyzed after two weeks of drug withdrawal. *n*=4
1016 independent experiments. Scale bar, 100 µm. **B**, Quantification of organoid morphology (granular,
1017 mid, cystic) in each condition at 14 days. ***p<0.001; ****p<0.0001 (Two-way ANOVA, granular
1018 vs. control); #p<0.05; ####p<0.0001 (cystic vs. control). **C**, Organoid size (µm) measured at 14
1019 days. *n*=80–100 organoids/condition across 4 experiments; ****p<0.0001 (One-way ANOVA). **D**,
1020 Confocal images of organoids stained for CK14 (green) and CK8/18 (red), showing marker
1021 changes 2 weeks after treatment. DAPI (blue) stains nuclei; bottom panels show merged IF and
1022 brightfield images. *n*=4. Scale bar, 100 µm. **E**, Quantification of collective-migratory projection
1023 area (µm²) in all conditions at 2 weeks. *n*=25–30 organoids/condition; **p<0.01 (unpaired
1024 Student's *t*-test). **F**, Number of secondary organoids formed from single-cell dissociation
1025 (indicating self-renewal) at 21 days. *n*=3 independent experiments; *p<0.05; **p<0.01 (One-way
1026 ANOVA).
1027
1028 **Figure 5. THC and SR2 trigger early and reversible epigenetic remodeling, followed by later**
1029 **differentiation. A,** Schematic timeline of the experimental workflow. **B**, Volcano plots showing
1030 differentially expressed genes in organoids treated with THC (10 nM) or SR2 (100 nM) vs. vehicle
1031 at day 3 and day 14 post-treatment. Genes with $\log_2$ fold change between −1 and 1 are
1032 considered unchanged. *n*=3 independent experiments. **C,** Gene Ontology (GO) enrichment
1033 analysis at day 3 of treatment, showing epigenetic regulation pathways significantly altered in
1034 SR2-treated organoids compared to control. Normalized Enrichment Score (NES) and gene set

size are indicated. **D,** Gene Set Enrichment Analysis (GSEA) of pathways related to pluripotency (top) and Polycomb Repressive Complex 2 (PRC2; bottom) in SR2-treated vs. control organoids at day 3 of treatment. **E,** Dot plots showing KEGG pathway enrichment analysis of differentially expressed genes following THC (top) or SR2 (bottom) treatment and evaluated at day 14, providing rationale for therapeutic tamoxifen combination in ***Figure 7***. **F,** Violin plots showing expression scores of validated UTF1 (top) and PRC2 (bottom) targets at day 3 (32). **G,** Violin plots of the same gene sets as in (E) at day 14 post-treatment (32). **H-I,** Organoids stained for H3K9me3 (red) and phalloidin (cytoskeleton marker; yellow) in upper images; H3K4me3 (red), H3K27me3 (green) and phalloidin (yellow) in bottom images, at day 3 (**H**) and day 14 (**I**), with DAPI (blue) staining nuclei. Violin plots show quantification of total nuclear fluorescence intensity per nucleus (800-1500 nuclei were evaluated per condition) for every staining, and the H3K27me3/H3K4me3 ratio denotes chromatin bivalency. *n*=3 independent experiments. Scale bar, 100 µm.

Figure 6. THC and SR2 promote stable differentiation, remodeling organoid architecture, migration, and cytokine signaling in a 3D co-culture system under shear stress. A, Schematic of the experimental setup. Organoids embedded in BME were co-cultured with cancer-associated fibroblasts (CAFs) and exposed to circulating peripheral blood mononuclear cells (PBMCs), with continuous pumped flux inducing shear stress. Co-cultures were treated with vehicle, THC (10 nM), or SR2 (100 nM) for 4 days, followed by 10 days in drug-free media. Samples were analyzed at two time points as indicated. **B,** Quantification of organoid morphology (granular, mid, cystic) at day 10 across conditions. *n*=3 independent experiments; *p<0.05 vs. control (granular); $^{\#}$p<0.05 vs. control (cystic) (Two-way ANOVA). **C,** Organoid size (µm) measured at day 4 and day 10. *n*=3 independent experiments; **p<0.01; ***p<0.001; ****p<0.0001 (One-way ANOVA). **D,** Percentage of organoids exhibiting collective migration at day 4 and day 10 in each treatment condition. *n*=3 independent experiments; **p<0.01 (One-way ANOVA). **E,** Quantification of collective migratory projection area (µm²) across conditions at day 4 and day 10. *n*=3 independent experiments; **p<0.01 (One-way ANOVA). **F,** Streptavidin-HRP based analysis of cytokines and chemokines secreted into the culture medium at day 10 for each condition: PBMC alone (red) or organoids+PBMCs+CAFs treated with vehicle (yellow), THC

1065 (green) or SR2 (blue). *n*=3 independent experiments; **p<0.01 (One-way ANOVA). **G-H,** Confocal
1066 images of organoids at day 10 stained for H3K4me3 (red) and phalloidin (yellow) (**G**) and for
1067 H3K27me3 (green) and phalloidin (yellow) (**H**), with DAPI (blue) marking nuclei. Violin plots show
1068 the quantification of total nuclear fluorescence intensity per nucleus (800-1500 nuclei were
1069 evaluated per condition) for every staining, as indicated. *n*=3 independent experiments. Scale
1070 bar, 100 µm.
1071
1072 **Figure 7. Cannabinoid-induced differentiation enhances tamoxifen response by promoting**
1073 **basal-to-luminal switching and reducing tumor organoid fitness. A,** Schematic of the
1074 experimental design. MMTV-PyMT–derived organoids were pre-treated with vehicle, THC (10
1075 nM), or SR2 (100 nM) for 4 days, followed by 10 days in drug-free media. Tamoxifen (0.5 µM)
1076 was then administered for 4 days, and cultures were analyzed immediately or up to 2 weeks later.
1077 **B,** Flow cytometry analysis of apoptosis using PI and Annexin V, assessed immediately after
1078 tamoxifen exposure or 2 weeks later in pre-differentiated cultures. *n*=4 independent experiments;
1079 *p<0.05; **p<0.01; (Unpaired Student's t-test). **C,** Cell cycle profiles comparing tamoxifen alone
1080 to SR2 + tamoxifen at increasing doses (0–5 µM). Left: representative flow cytometry plots. Right:
1081 quantification of cell cycle phases (G1, S, G2/M). *n*=3 independent experiments. **D,** Quantification
1082 of organoid morphology at endpoint: granular (basal), mid-transition, or cystic (luminal). *n*=4
1083 independent experiments; **p<0.01; ***p<0.001 ****p<0.0001 (Two-way ANOVA). **E,** Organoid
1084 size (µm) at endpoint across treatment conditions. *n*=4; 80–100 organoids per condition; *p<0.05;
1085 **p<0.01; ****p<0.0001 (One-way ANOVA). **F,** Percentage of organoids exhibiting collective-
1086 migratory projections at endpoint. *n*=4; *p*-values as indicated (One-way ANOVA). **G,** Self-renewal
1087 capacity assessed by quantification of secondary organoids formed after single-cell dissociation.
1088 *n*=4 independent experiments; **p<0.01; ***p<0.001; ****p<0.0001 (One-way ANOVA).
1089
1090 **Figure 8. CB2R–tamoxifen combination enhances therapy efficacy in patient-derived**
1091 **breast cancer organoids**. **A**, Experimental workflow. Surgical specimens were used to establish
1092 patient-derived organoid cultures. After expansion, organoids were treated with vehicle or SR2
1093 (100 nM) for 4 days, followed by a 10-day drug-free period. Prior to tamoxifen treatment, cell
1094 dispersal from organoids was assessed using dynamic holographic imaging. Tamoxifen (5 µM)

1095 was then administered for 4 days. Organoids were analyzed two weeks later to evaluate
1096 cooperative effects on self-renewal. *n*=2 independent tumors, 3 technical replicates each. **B**,
1097 Representative holographic images showing 2D movement of organoid-derived cells treated with
1098 vehicle or SR2 (100 nM), assessed in a wound healing assay at different time points. **C–F**,
1099 Quantification of wound healing assay parameters: cell area (μm²) (**C**), irregularity (**D**), migration
1100 distance (μm) (**E**), and motility (μm) (**F**) under both treatment conditions. A linear model was fitted
1101 to assess the impact of experimental conditions on each variable. Statistics shown in **Supp.**
1102 **Figure 8**. **G**, Confocal images of organoids stained for E-cadherin (green) and Snail (red),
1103 analyzed 10 days post-differentiation. Nuclei were stained with DAPI (blue). Shown are
1104 representative 3D confocal stacks. Scale bar = 100 μm. **H**, Quantification of organoid size (μm)
1105 at day 10 post-differentiation. ****$p < 0.0001$ (one-way ANOVA). **I**, Percentage of organoids
1106 displaying collective migration at day 10 post-differentiation. **J**, Total number of secondary
1107 organoids formed after single-cell disaggregation, reflecting self-renewal capacity, measured two
1108 weeks after tamoxifen treatment. ***$p < 0.001$ (one-way ANOVA). **K**, Representative brightfield
1109 images of organoids at different time points: 10 days after differentiation, and 5 or 20 days after
1110 tamoxifen treatment, following the experimental timeline shown in (A).

Figure 1

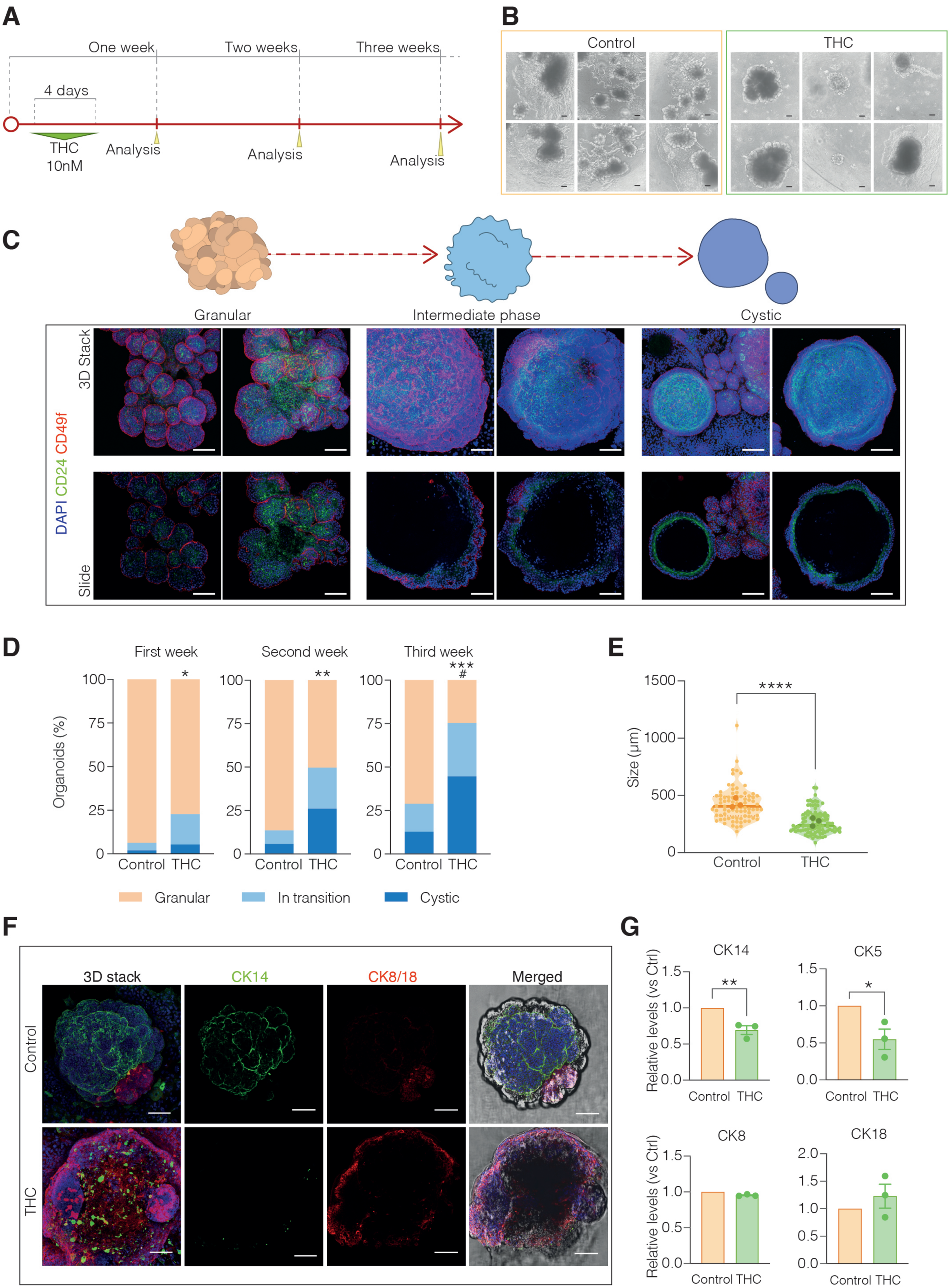
A
One week
Two weeks
Three weeks
4 days
THC
10nM
Analysis
Analysis
Analysis
B
Control
THC
C
Granular
Intermediate phase
Cystic
3D Stack
Slide
DAPI CD24 CD49f
D
First week
Second week
Third week
Organoids (%)
100
75
50
25
0
Control THC
*
**
***
#
Granular
In transition
Cystic
E
1500
1000
500
0
Size (µm)
****
Control
THC
F
3D stack
CK14
CK8/18
Merged
Control
THC
G
CK14
CK5
CK8
CK18
Relative levels (vs Ctrl)
1.5
1.0
0.5
0.0
2.0
**
*
Control THC

Figure 2

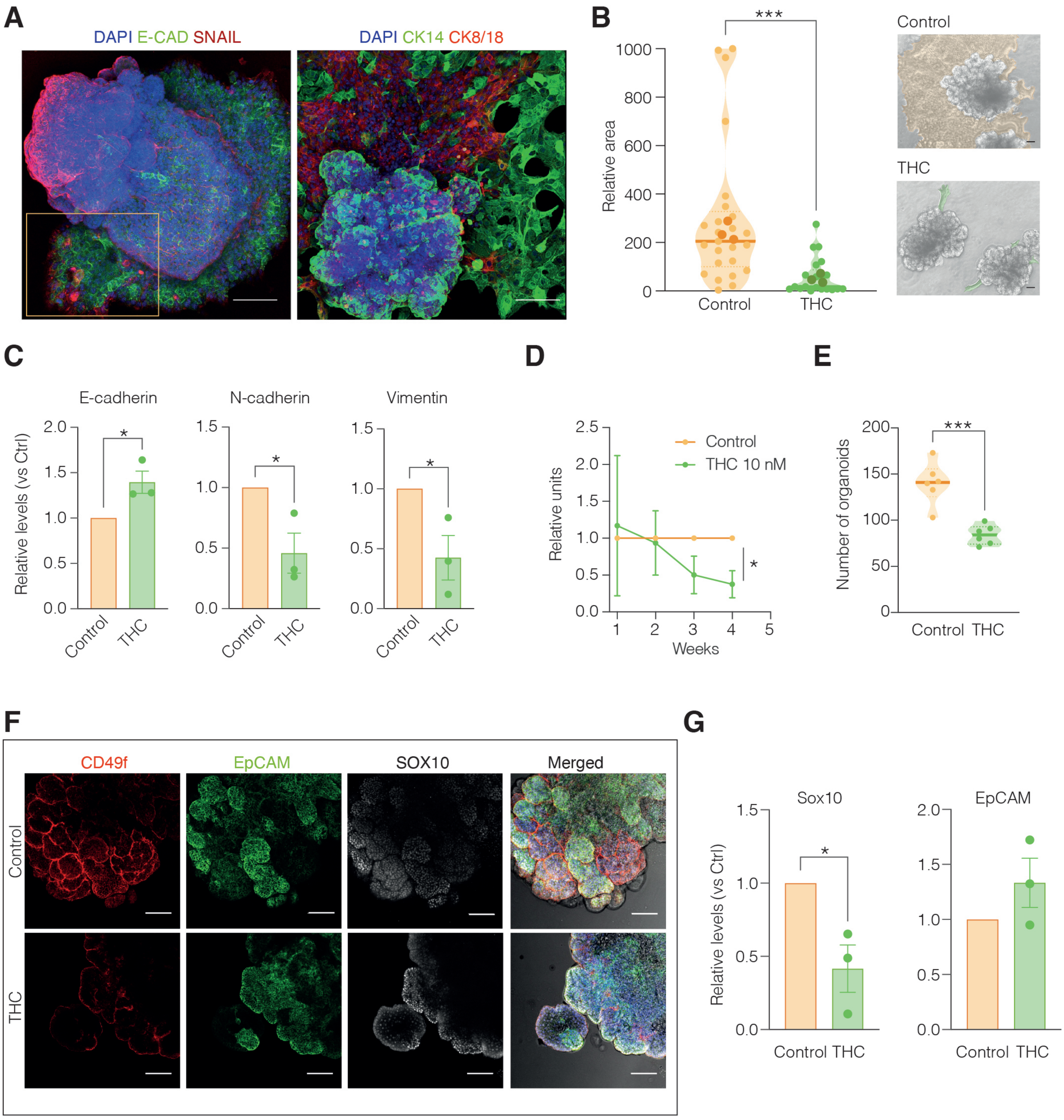
A
DAPI E-CAD SNAIL
DAPI CK14 CK8/18
B
***
Relative area
1000
800
600
400
200
0
Control
THC
Control
THC
C
E-cadherin
N-cadherin
Vimentin
Relative levels (vs Ctrl)
2.0
1.5
1.0
0.5
0.0
*
Control
THC
D
Relative units
Control
THC 10 nM
Weeks
1
2
3
4
5
E
Number of organoids
200
150
100
50
0
***
Control THC
F
CD49f
EpCAM
SOX10
Merged
Control
THC
G
Sox10
EpCAM
Relative levels (vs Ctrl)
Control THC

Figure 3

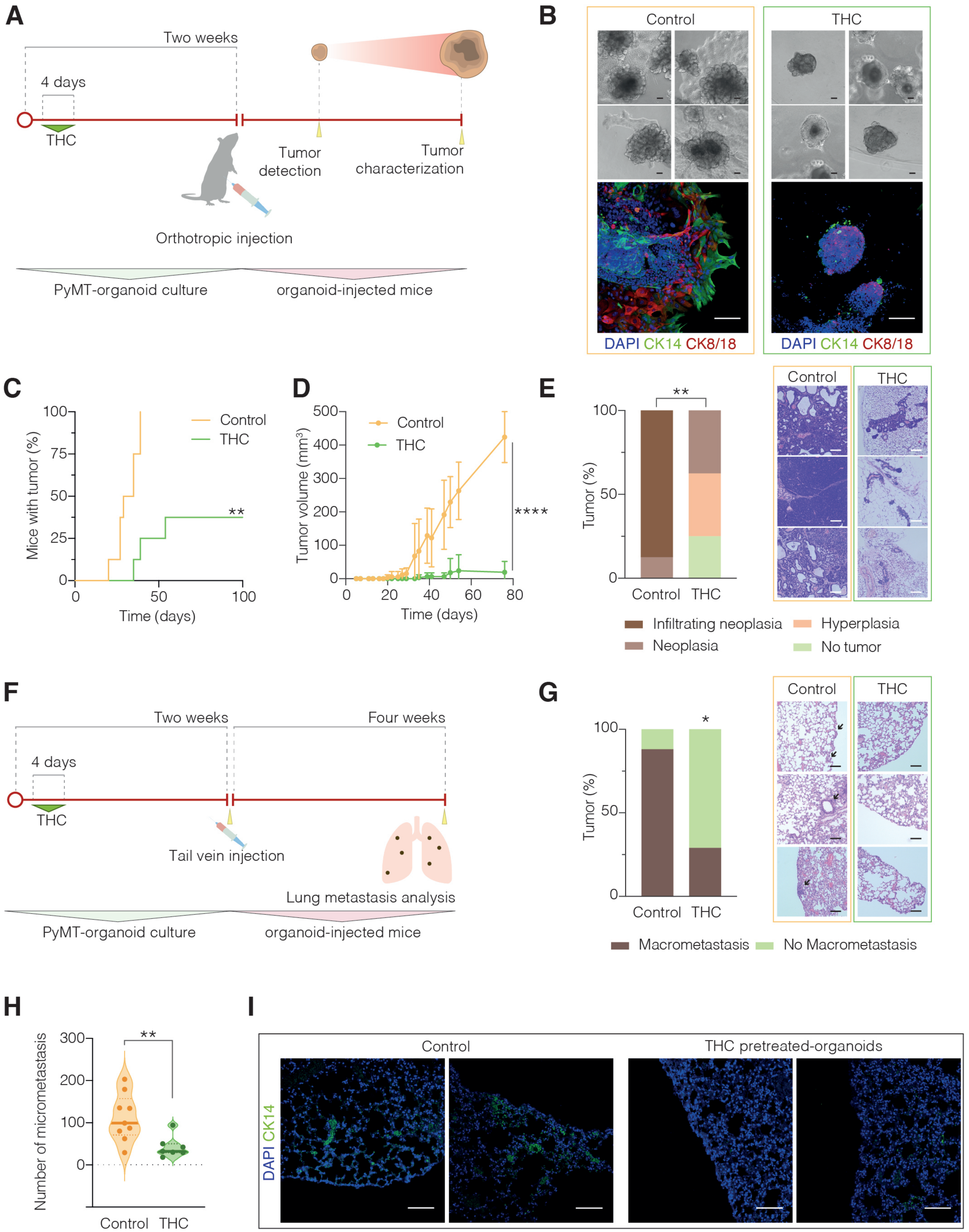
A
Two weeks
4 days
THC
Tumor detection
Tumor characterization
Orthotropic injection
PyMT-organoid culture
organoid-injected mice
B
Control
THC
DAPI CK14 CK8/18
C
Mice with tumor (%)
Control
THC
**
Time (days)
D
Tumor volume (mm³)
Control
THC
****
Time (days)
E
Tumor (%)
**
Control THC
Infiltrating neoplasia
Hyperplasia
Neoplasia
No tumor
F
Two weeks
Four weeks
4 days
THC
Tail vein injection
Lung metastasis analysis
PyMT-organoid culture
organoid-injected mice
G
Tumor (%)
*
Control THC
Macrometastasis
No Macrometastasis
H
Number of micrometastasis
**
Control THC
I
Control
THC pretreated-organoids
DAPI CK14

Figure 4

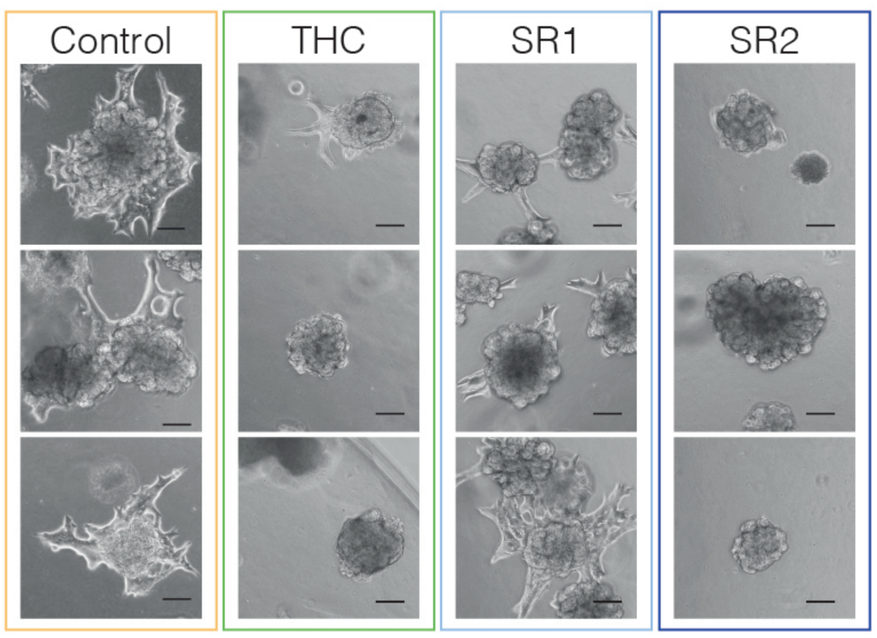
A
Control
THC
SR1
SR2

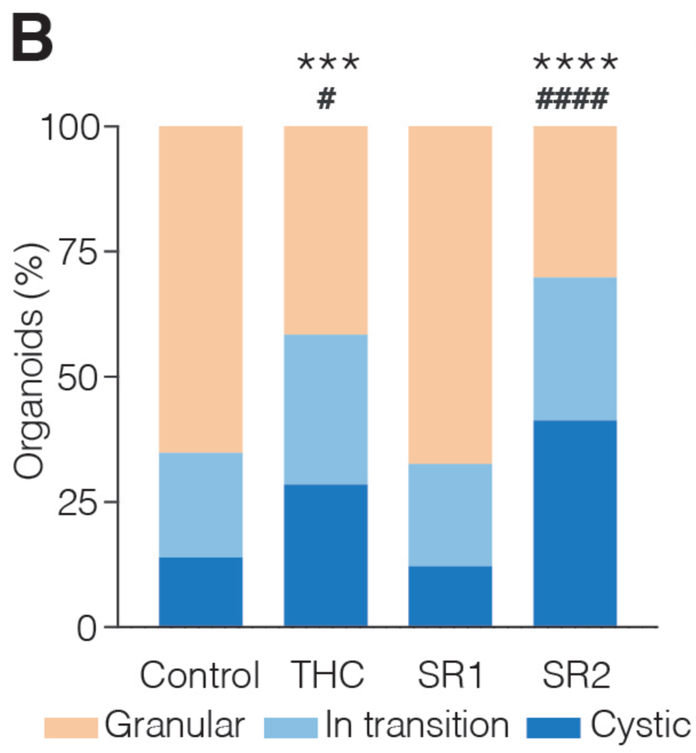
B
***
#
****
####
100
75
50
25
0
Organoids (%)
Control
THC
SR1
SR2
Granular
In transition
Cystic

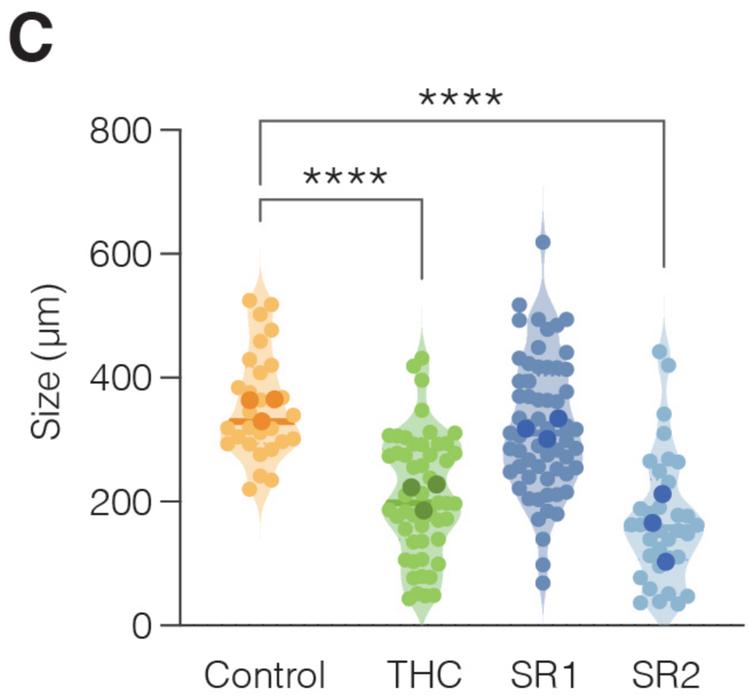
C
****
****
800
600
400
200
0
Size (µm)
Control
THC
SR1
SR2

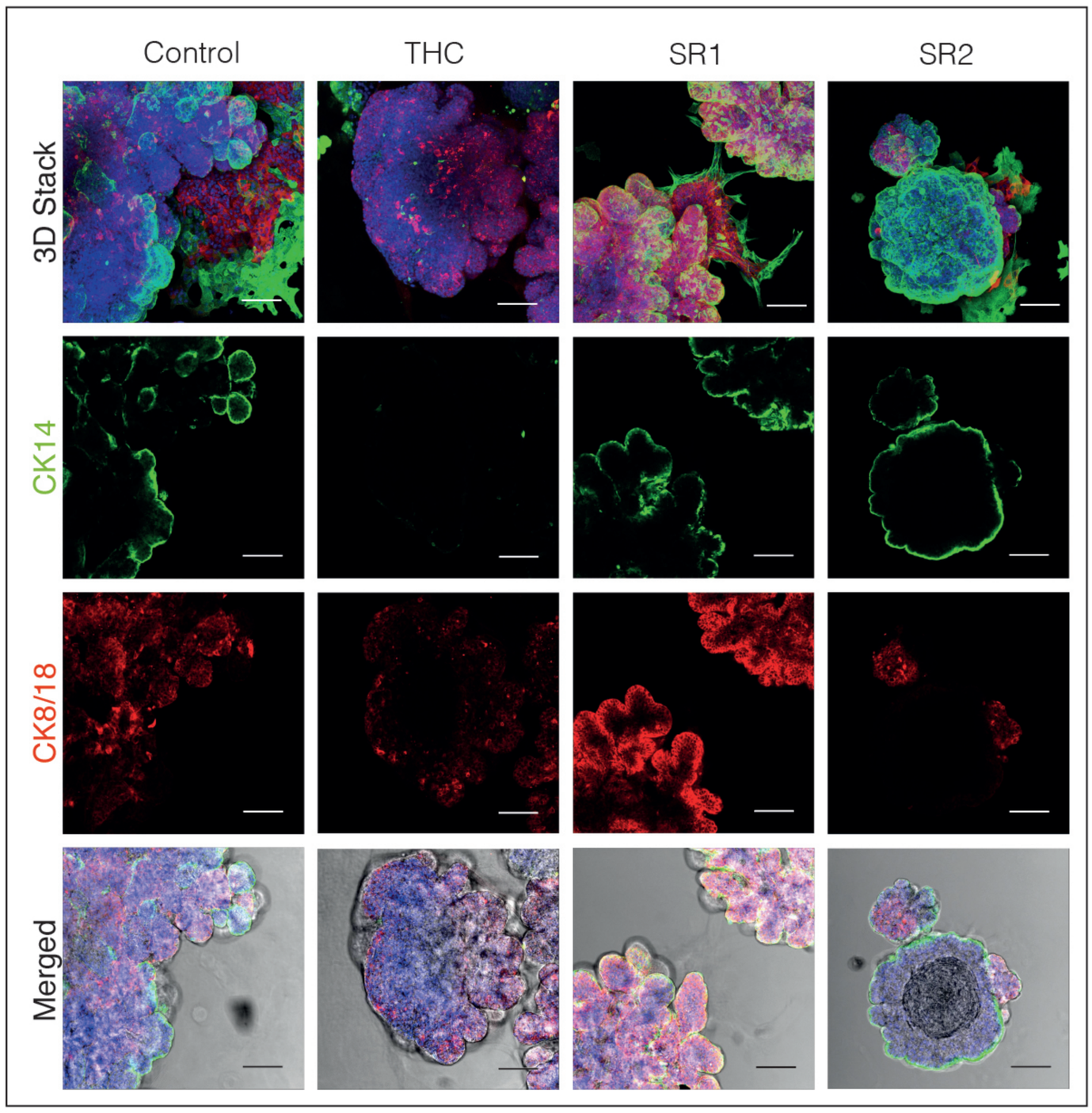
D
Control
THC
SR1
SR2
3D Stack
CK14
CK8/18
Merged

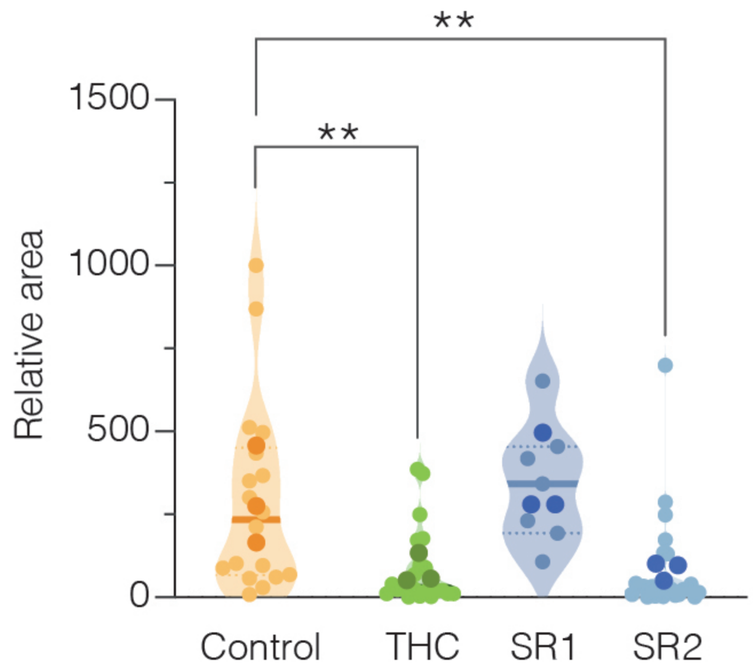
E
**
**
1500
1000
500
0
Relative area
Control
THC
SR1
SR2

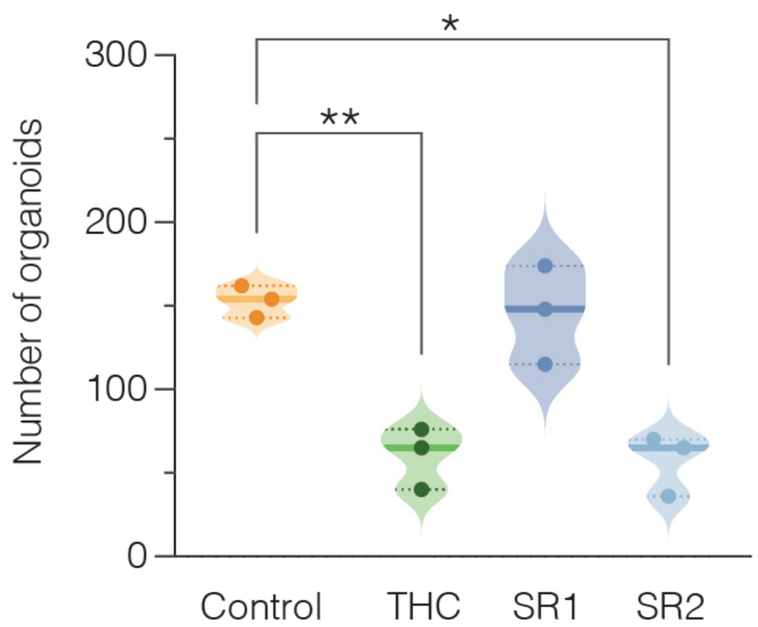
F
*
**
300
200
100
0
Number of organoids
Control
THC
SR1
SR2

Figure 5

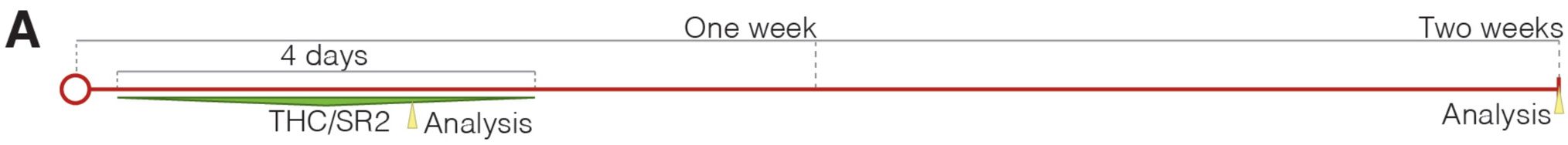

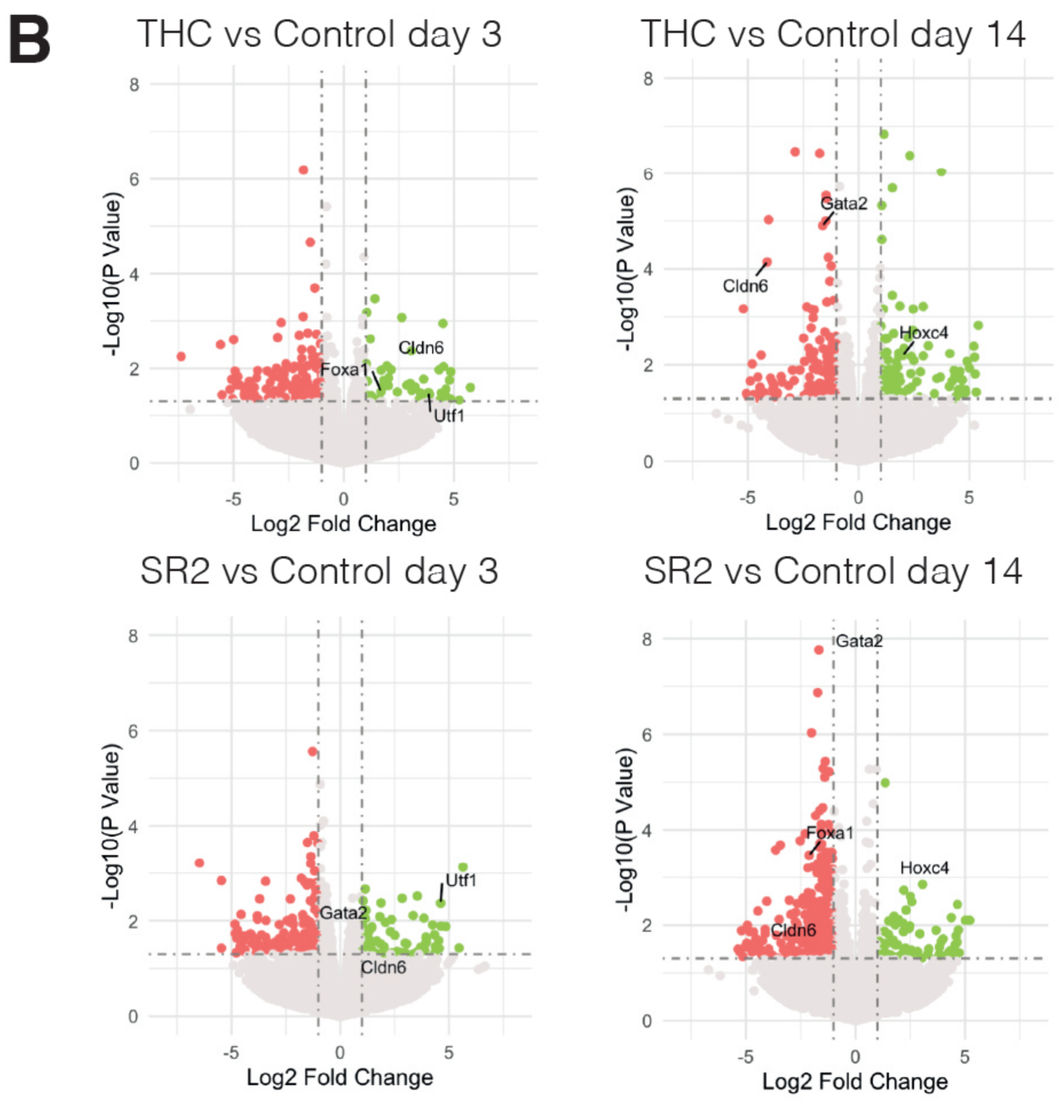

C Control enrichment sets vs SR2

Day 3	NES	Size
N-acetyltransferase activity	-2.00	78
N-acyltransferase activity	-1.89	94
Acetyltransferase activity	-1.81	99
Peptide n-acetyltransferase activity	-1.80	64
Histone exchange	-1.66	16
Histone acetyltransferase activity	-1.54	56
Histone H3K9 modification	-1.53	43
Cromatin silencing	-1.53	60
Histone binding	-1.49	174
Histone H3K9 methylation	-1.49	119
Methylation dependent protein binding	-1.43	62

D Gene Set Enrichment Analysis during SR2 treatment (day 03)

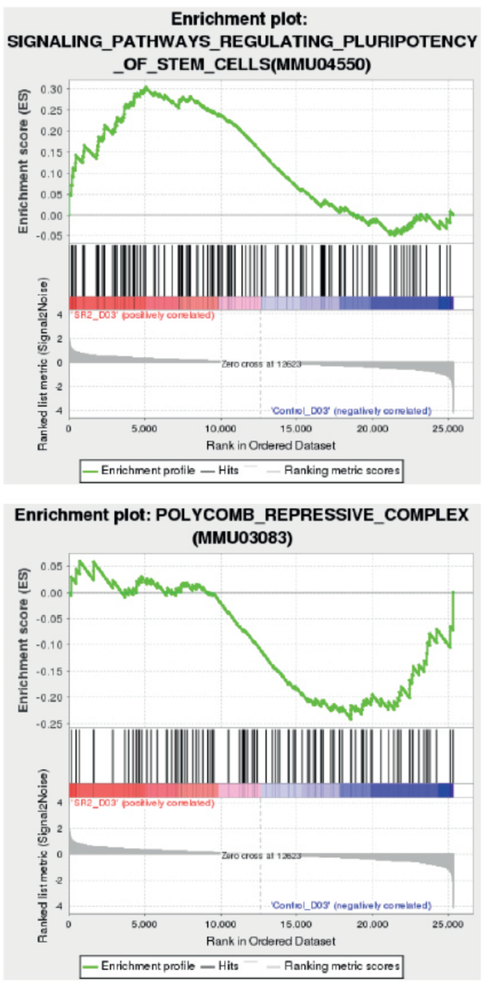

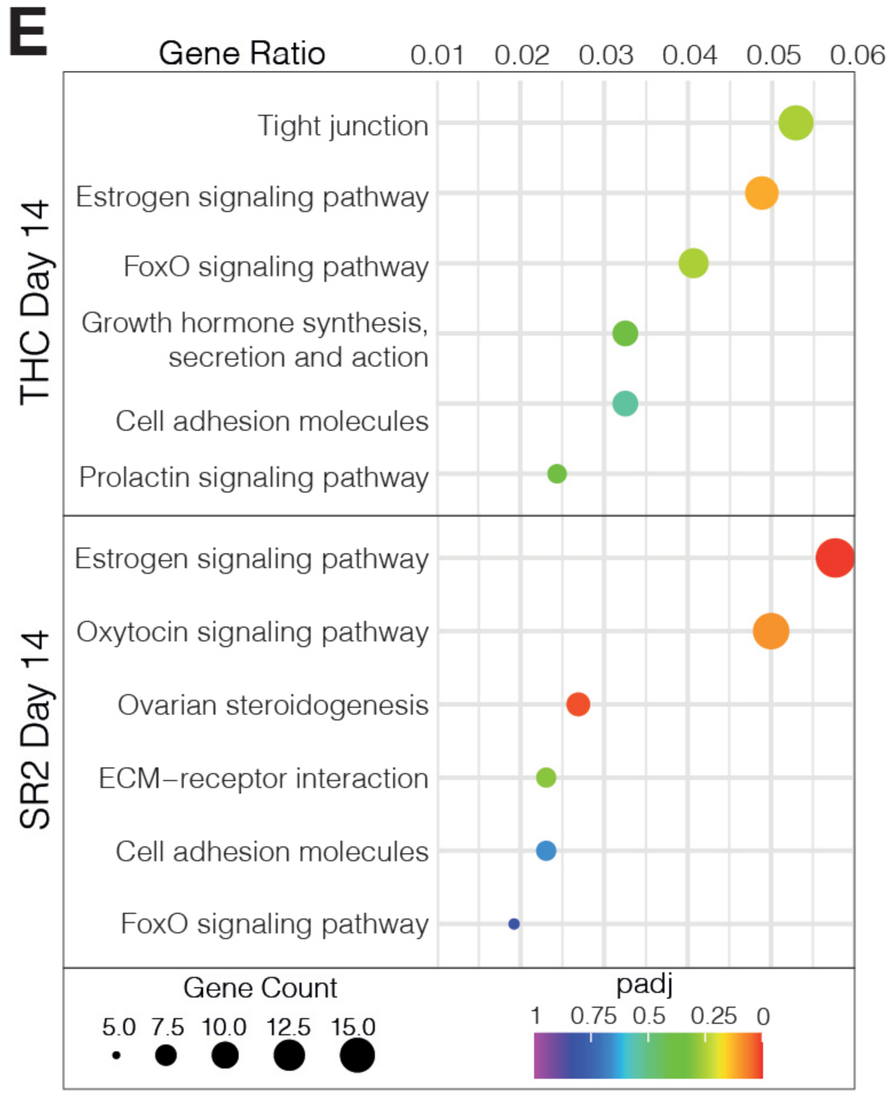

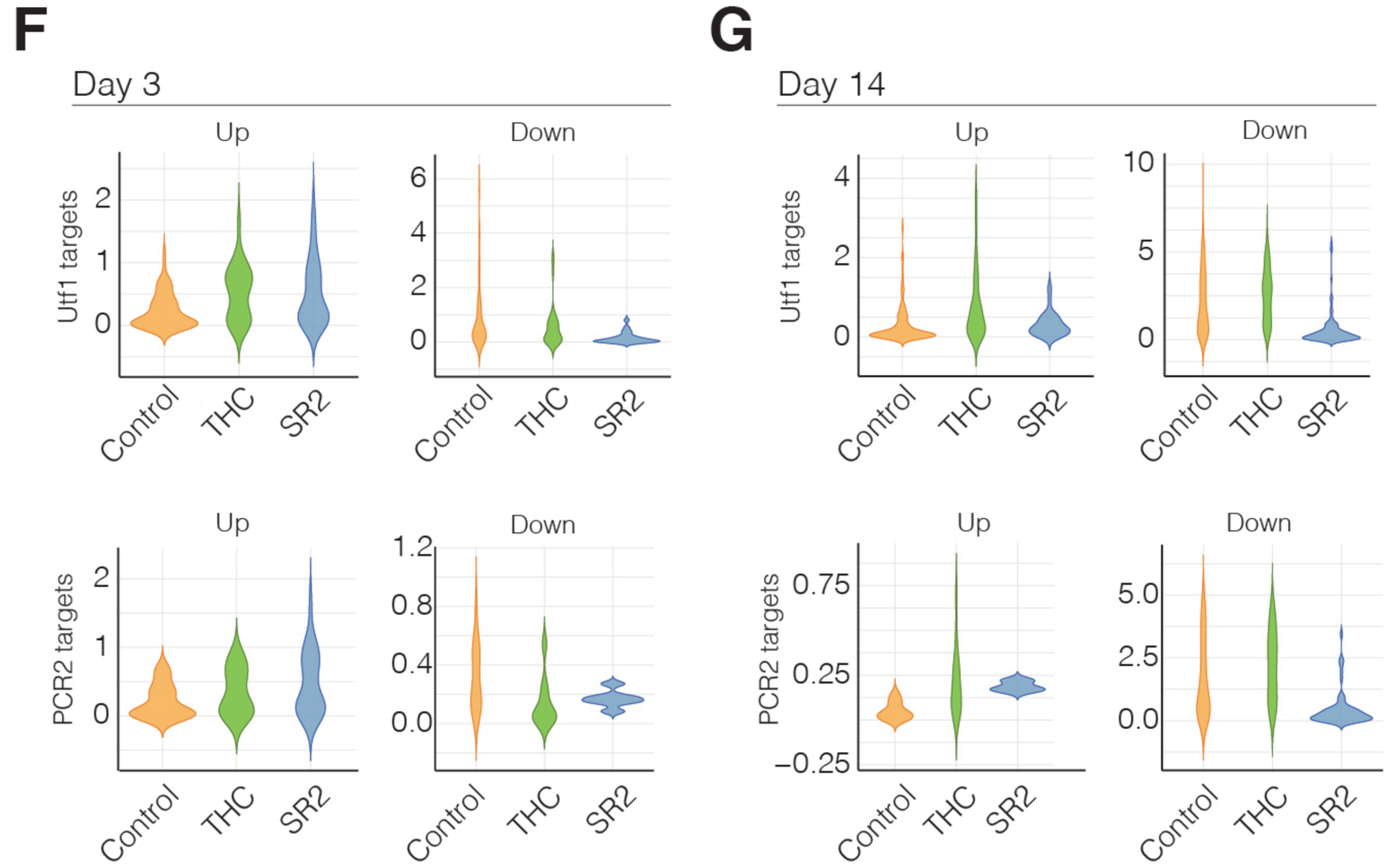

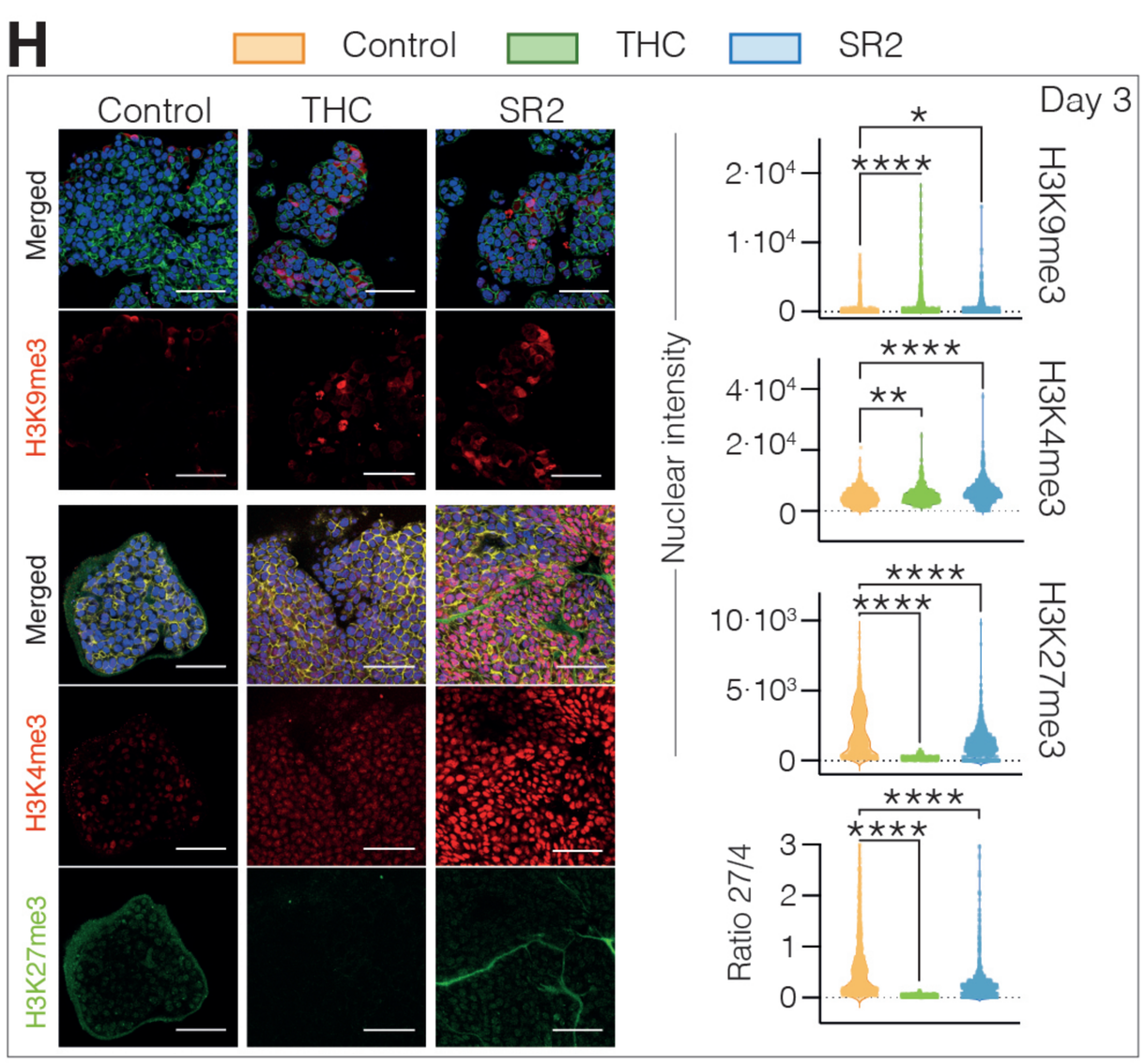

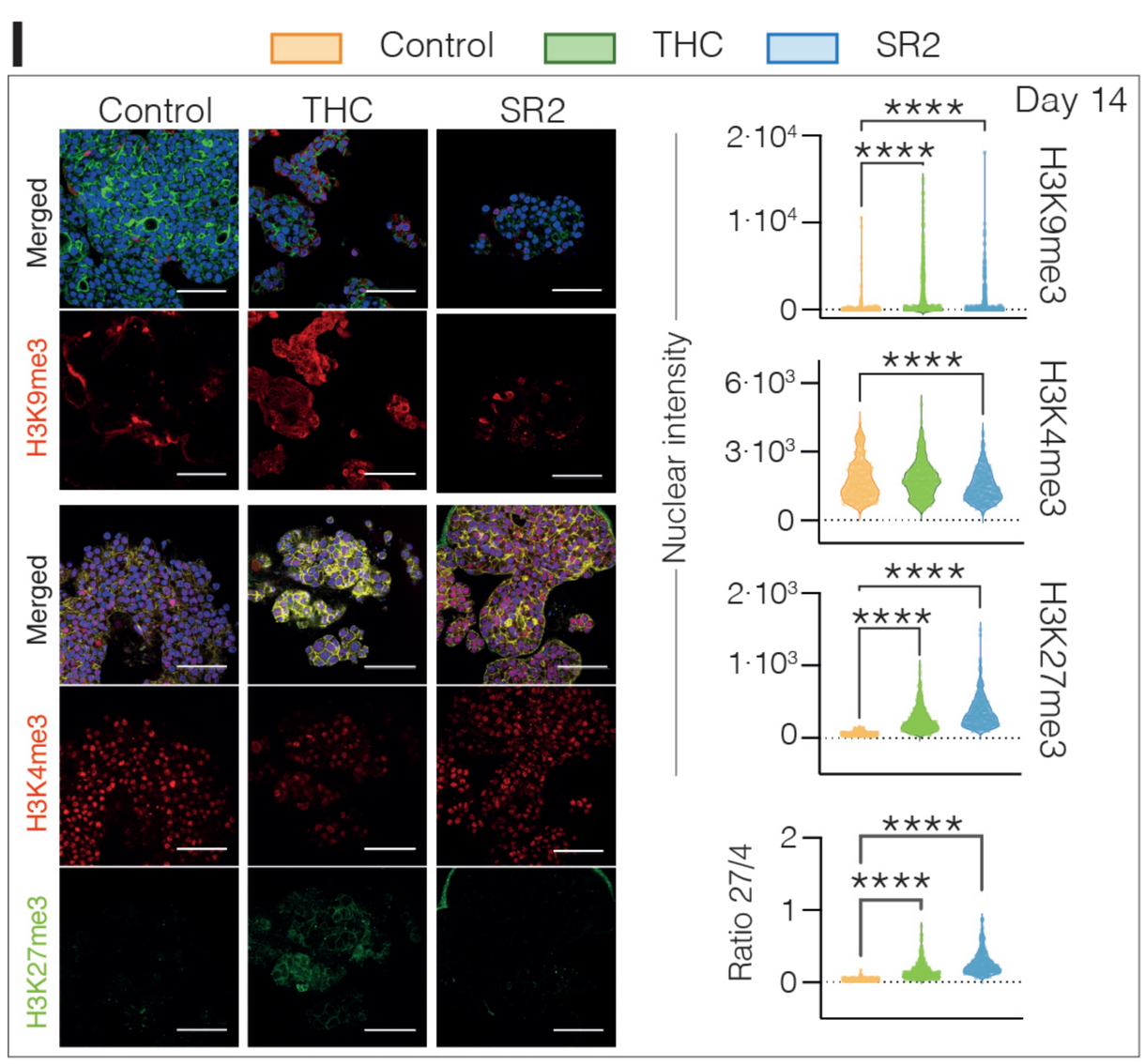

Figure 6

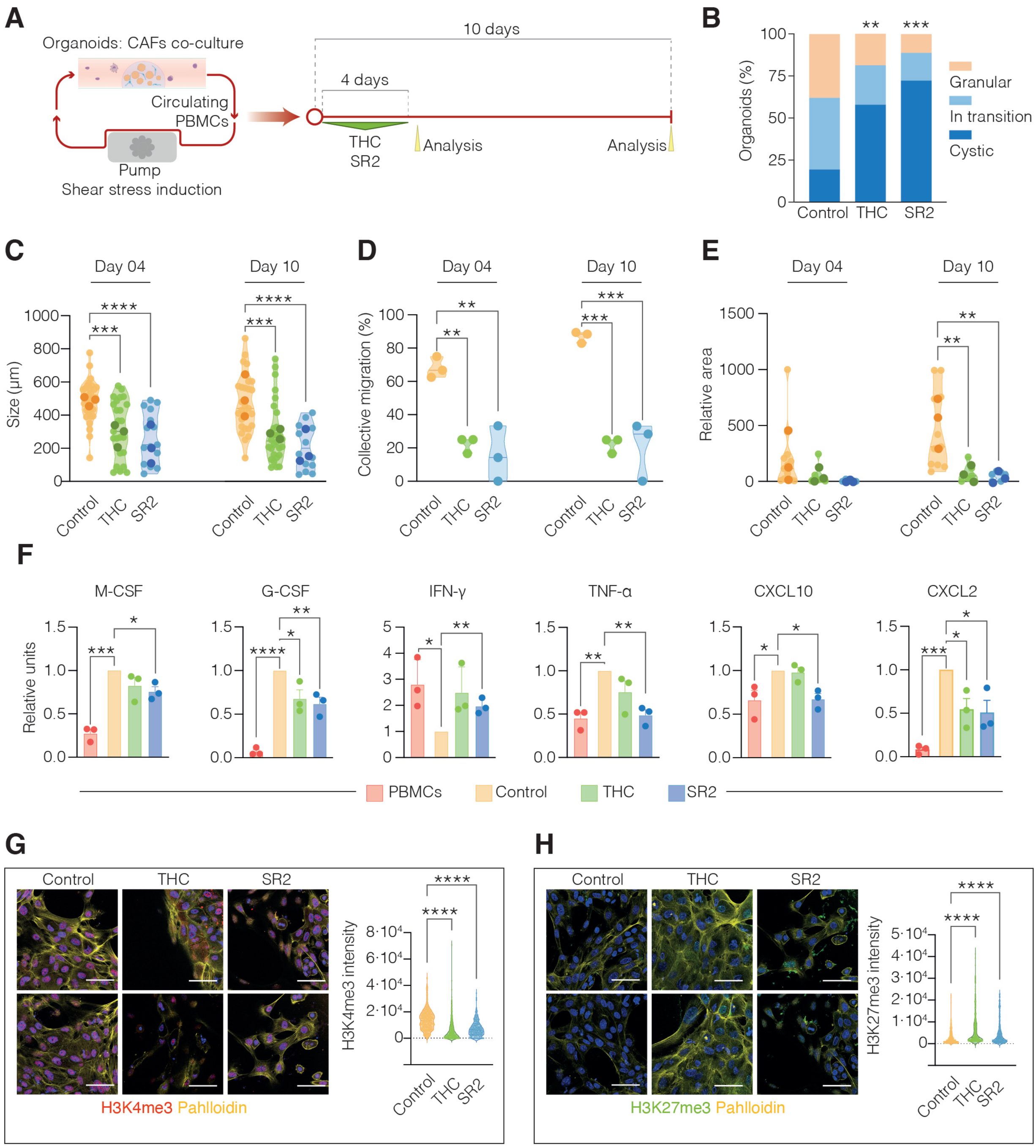
A
Organoids: CAFs co-culture
Circulating PBMCs
Pump
Shear stress induction
10 days
4 days
THC
SR2
Analysis
Analysis
B
Organoids (%)
Granular
In transition
Cystic
Control
THC
SR2
C
Day 04
Day 10
Size (µm)
D
Collective migration (%)
E
Relative area
F
M-CSF
G-CSF
IFN-γ
TNF-α
CXCL10
CXCL2
Relative units
PBMCs
Control
THC
SR2
G
H3K4me3 Pahlloidin
H3K4me3 intensity
H
H3K27me3 Pahlloidin
H3K27me3 intensity

Figure 7

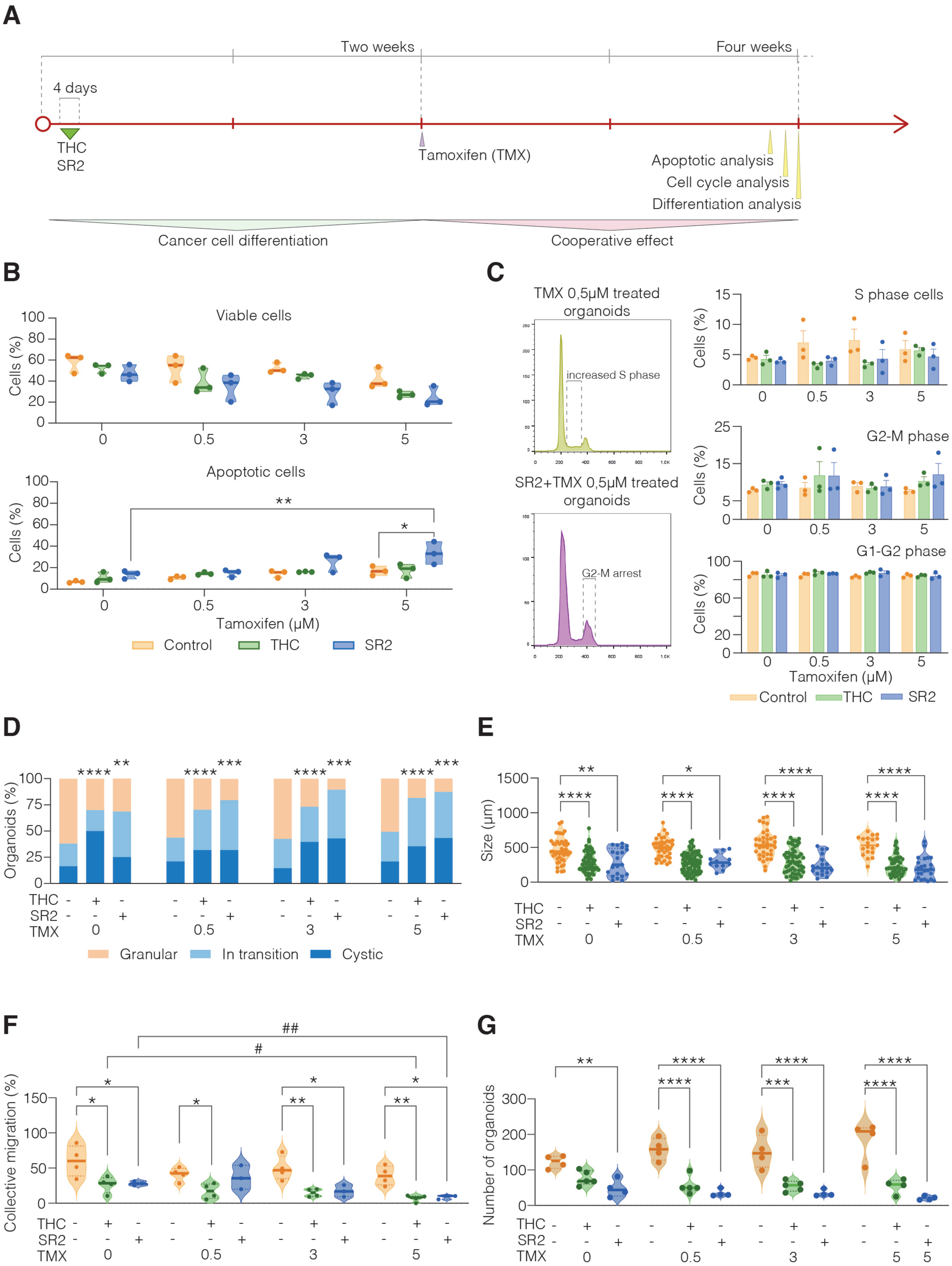
A
Two weeks
Four weeks
4 days
THC
SR2
Tamoxifen (TMX)
Apoptotic analysis
Cell cycle analysis
Differentiation analysis
Cancer cell differentiation
Cooperative effect
B
Viable cells
Cells (%)
Apoptotic cells
Tamoxifen (μM)
Control
THC
SR2
C
TMX 0,5μM treated organoids
increased S phase
SR2+TMX 0,5μM treated organoids
G2-M arrest
S phase cells
G2-M phase
G1-G2 phase
D
Organoids (%)
Granular
In transition
Cystic
E
Size (μm)
F
Collective migration (%)
G
Number of organoids

Figure 8

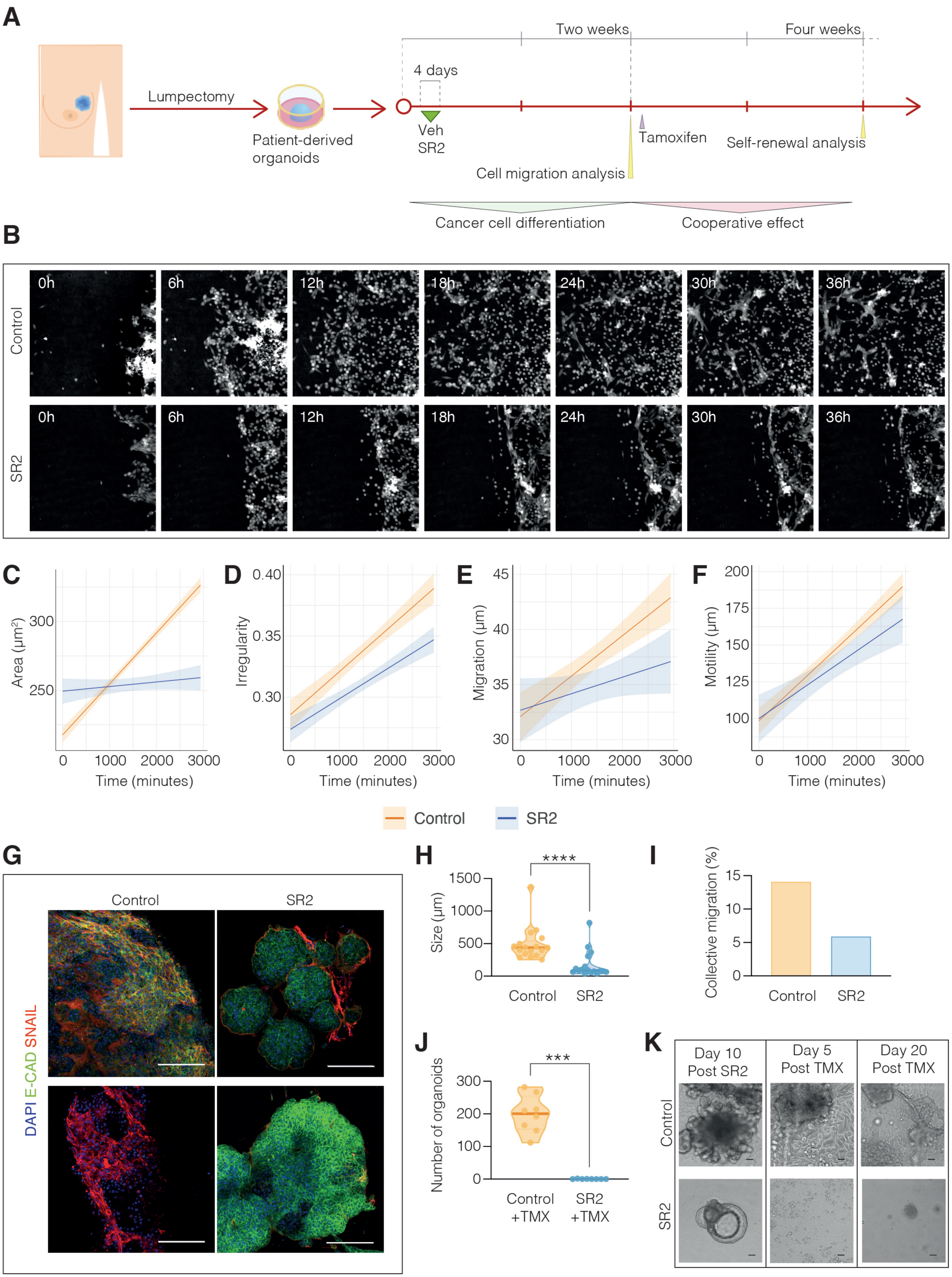
A
Lumpectomy
Patient-derived organoids
4 days
Veh
SR2
Two weeks
Four weeks
Tamoxifen
Self-renewal analysis
Cell migration analysis
Cancer cell differentiation
Cooperative effect
B
Control
SR2
0h
6h
12h
18h
24h
30h
36h
C
Area (µm²)
Time (minutes)
D
Irregularity
Time (minutes)
E
Migration (µm)
Time (minutes)
F
Motility (µm)
Time (minutes)
Control
SR2
G
Control
SR2
DAPI E-CAD SNAIL
H
Size (µm)
****
Control
SR2
I
Collective migration (%)
Control
SR2
J
Number of organoids
***
Control +TMX
SR2 +TMX
K
Day 10 Post SR2
Day 5 Post TMX
Day 20 Post TMX
Control
SR2